iScience

CellPress
OPEN ACCESS

Article

AP39 through AMPK-ULK1-FUNDC1 pathway regulates mitophagy, inhibits pyroptosis, and improves doxorubicin-induced myocardial fibrosis

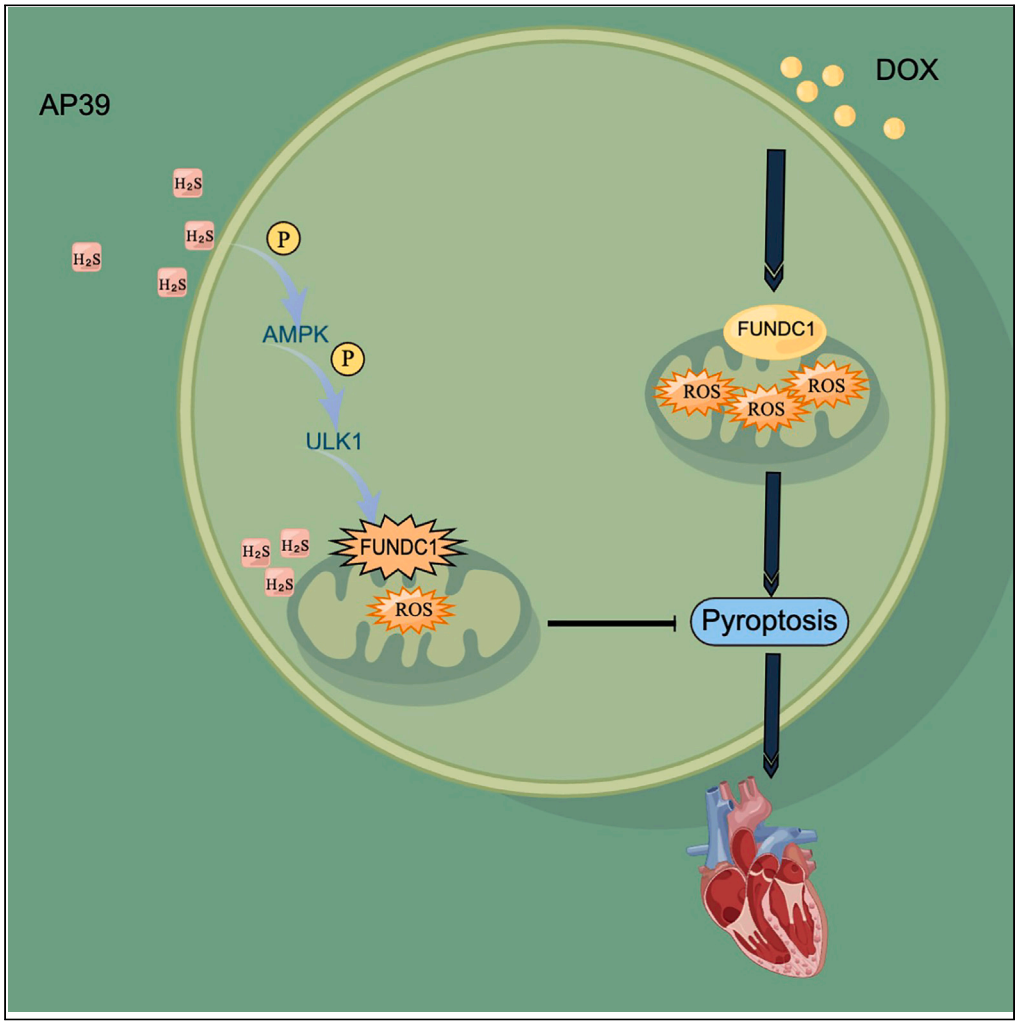

Junxiong Zhao, Ting Yang, Jiali Yi, ..., Maojun Liu, Chun Chu, Jun Yang

1996020012@usc.edu.cn (C.C.)
2018010473@usc.edu.cn (J.Y.)

Highlights

AMPK-ULK1-FUNDC1 pathway could be an important target for doxorubicin-induced cardiomyopathy

AP39 may regulate mitophagy and pyroptosis to improve myocardial fibrosis

AP39 through AMPK-ULK1-FUNDC1 regulates mitophagy and pyroptosis

Zhao et al., iScience 27, 109321
April 19, 2024
https://doi.org/10.1016/j.isci.2024.109321

iScience

CellPress
OPEN ACCESS

Article

AP39 through AMPK-ULK1-FUNDC1 pathway regulates mitophagy, inhibits pyroptosis, and improves doxorubicin-induced myocardial fibrosis

Junxiong Zhao,[1,5] Ting Yang,[2,3,5] Jiali Yi,[4,5] Hongmin Hu,[1] Qi Lai,[2,3] Liangui Nie,[1] Maojun Liu,[1] Chun Chu,[3,*] and Jun Yang[1,6,*]

SUMMARY

Doxorubicin induces myocardial injury and fibrosis. Still, no effective interventions are available. AP39 is an H_2S donor that explicitly targets mitochondria. This study investigated whether AP39 could improve doxorubicin-induced myocardial fibrosis. Doxorubicin induced significant myocardial fibrosis while suppressing mitophagy-related proteins and elevating pyroptosis-related proteins. Conversely, AP39 reverses these effects, enhancing mitophagy and inhibiting pyroptosis. *In vitro* experiments revealed that AP39 inhibited H9c2 cardiomyocyte pyroptosis, improved doxorubicin-induced impairment of mitophagy, reduced ROS levels, ameliorated the mitochondrial membrane potential, and upregulated AMPK-ULK1-FUNDC1 expression. In contrast, AMPK inhibitor (dorsomorphin) and ULK1 inhibitor (SBI-0206965) reversed AP39 antagonism of doxorubicin-induced FUNDC1-mediated impairment of mitophagy and secondary cardiomyocyte pyroptosis. These results suggest that mitochondria-targeted H_2S can antagonize doxorubicin-induced pyroptosis and impaired mitophagy in cardiomyocytes via AMPK-ULK1-FUNDC1 and ameliorated myocardial fibrosis and remodeling.

INTRODUCTION

Anthracycline antineoplastic drugs such as doxorubicin are first-line agents in oncology treatment. Still, the cardiotoxic effects and fibrosis of this drug limit its clinical utility. Clinical studies have found that doxorubicin induces congestive heart failure and cardiomyopathy associated with anthracycline doses.[1] Cardiomyocytes are highly susceptible to the effects of anthracyclines, which induce oxidative stress and programmed cardiomyocyte death, leading to myocardial fibrosis and cardiac dysfunction in mice.[2,3] Pyroptosis has recently been identified as a critical cause of doxorubicin-induced cardiotoxic effects, and cardiomyocyte pyroptosis promotes the progression of myocardial fibrosis and inflammatory responses.[4] Cardiomyocyte pyroptosis is one of the most essential forms of cardiomyocyte injury, and suppressing cardiomyocyte pyroptosis has been shown to improve the cardiotoxic effects of doxorubicin.[5] Cellular pyroptosis is a crucial target in doxorubicin-induced cardiomyopathy, but the role of cardiomyocyte pyroptosis in doxorubicin-associated cardiomyopathy and myocardial fibrosis is still not fully understood.

Mitophagy is a vital cellular activity and phenomenon for mitochondrial quality control, an important means of maintaining a certain number of healthy mitochondria in cardiomyocytes, and an important regulator of cardiomyocyte fate. Recent studies have found that defects in mitophagy can be an important cause of myocardial fibrosis.[6] In contrast, some studies have found that impaired mitophagy is also an important contributor to doxorubicin-induced cardiac injury,[7] with the majority of possible causes being related to the high production of reactive oxygen species and the large accumulation of damaged mitochondria.[8,9] Maintaining a moderate level of mitophagy is essential for maintaining cellular homeostasis and antagonizing the generation of cellular pyroptosis and is a key component in improving the myocardial fibrosis process.[10] Recently, FUNDC1-mediated mitophagy has been found to improve cardiac functional impairment due to lipotoxic cardiomyopathy by maintaining mitochondrial integrity.[11,12] Additionally, FUNDC1-mediated mitophagy can effectively reduce the production of reactive oxygen species (ROS) and inhibit myocardial fibrosis and cardiomyocyte hypertrophy.[13,14] Nonetheless, the relationship between FUNDC1-mediated mitophagy and doxorubicin-induced cardiomyopathy remains unclear.

H_2S (Hydrogen sulfide) is a gas signaling molecule recently discovered and is vital in cardiovascular physiological regulation. Recently, the myocardial tissue of rats with doxorubicin-induced cardiomyopathy with insufficient endogenous H_2S production may lead to cardiomyocyte

[1]Department of Cardiology, The First Affiliated Hospital, Hengyang Medical School, University of South China, Hengyang 421000, China
[2]School of Pharmaceutical Science of University of South China, Hengyang 421000, China
[3]Department of Pharmacy, The Second Affiliated Hospital, Hengyang Medical School, University of South China, Hengyang 421000, China
[4]Department of Cardiology, Hunan University of Medicine General Hospital, Huaihua 418000, China
[5]These authors contributed equally
[6]Lead contact
*Correspondence: 1996020012@usc.edu.cn (C.C.), 2018010473@usc.edu.cn (J.Y.)
https://doi.org/10.1016/j.isci.2024.109321

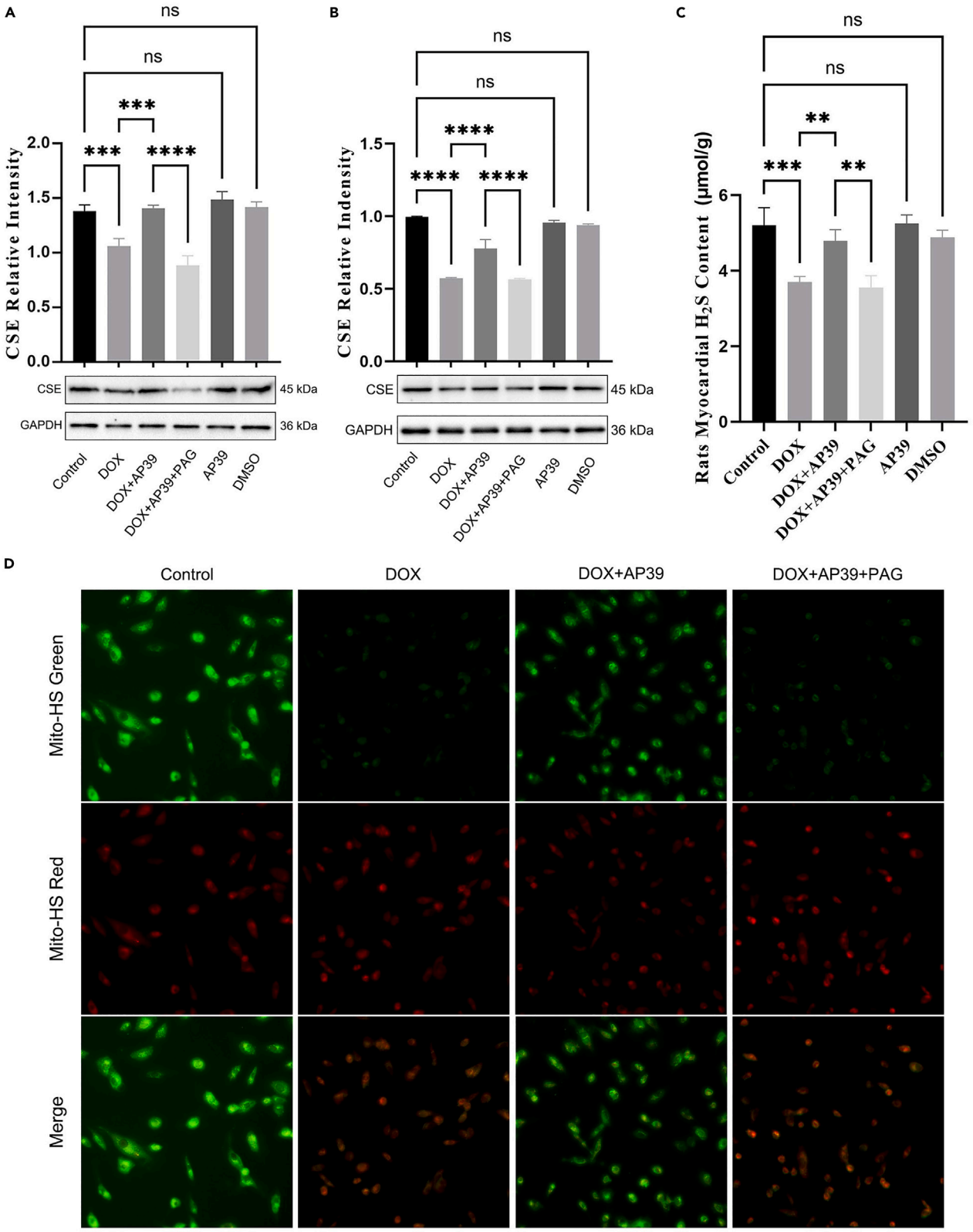
A
ns
ns
***
***
****
CSE Relative Intensity
2.0
1.5
1.0
0.5
0.0
CSE
45 kDa
GAPDH
36 kDa
Control
DOX
DOX+AP39
DOX+AP39+PAG
AP39
DMSO
B
ns
ns
****
****
****
CSE Relative Indensity
1.5
1.0
0.5
0.0
CSE
45 kDa
GAPDH
36 kDa
Control
DOX
DOX+AP39
DOX+AP39+PAG
AP39
DMSO
C
ns
ns
**
***
**
Rats Myocardial H2S Content (μmol/g)
6
4
2
0
Control
DOX
DOX+AP39
DOX+AP39+PAG
AP39
DMSO
D
Control
DOX
DOX+AP39
DOX+AP39+PAG
Mito-HS Green
Mito-HS Red
Merge

Figure 1. Effect of mitochondria-targeted H_2S on H_2S in DOX-treated myocardium

(A) Changes in the expression level of endogenous H_2S-producing enzyme CSE in rat myocardial tissue and its corresponding semiquantitative analysis by immunoblotting.

(B) Changes in the expression level of CSE in H9c2 cardiomyocytes and its corresponding semiquantitative analysis.

(C) Changes in H_2S content detected in rat myocardial tissue (μmol/g).

(D) Changes in the mitochondrial H_2S fluorescence signal detected by the mitochondrial H_2S probe. Green fluorescence is the excited state mitochondrial H_2S signal, and red fluorescence is the mitochondria. All experiments were independently replicated three times. Data were represented as mean ± SEM. **$p < 0.01$, ***$p < 0.001$, **** and $p < 0.0001$.

dysfunction and cause or aggravate apoptosis.[15] H_2S has been found to potentially inhibit the progression of myocardial fibrosis in rats. However, the underlying mechanism needs to be further elucidated.[16] Further studies have found that H_2S regulates the SIRT6/AMPK pathway to regulate autophagy in cardiomyocytes.[17] A study found that H_2S upregulates the AMPK/mTOR pathway to activate autophagy with increased phosphorylation of ULK1.[18]

Additionally, the AMPK/ULK1 pathway has been reported to potentially activate FUNDC1-mediated mitophagy.[19] Nonetheless, the regulatory relationship of H_2S with the AMPK-ULK1-FUNDC1 pathway is still unclear. AP39 is a targeted mitochondrial H_2S donor and a novel vehicle for specifically studying the effects of H_2S on mitochondrial physiological activity. AP39 has been shown to reduce ROS production without affecting mitochondrial respiratory complexes I and II and prevents myocardial reperfusion injury.[20] AP39 can also increase mitochondrial H_2S levels, restore mitochondrial membrane potential, improve mitochondrial swelling and damage caused by high glucose and lipids,[21] modulate mitochondrial dynamics to promote mitochondrial fusion effects, and increase cellular bioenergetics and cell viability.[22] However, the impact of AP39 on antineoplastic drug-associated cardiomyopathy and its underlying mechanisms remain unclear, and further studies are needed to determine whether there is a regulatory relationship with the AMPK-ULK1-FUNDC1 pathway.

In this study, a rat model of doxorubicin-induced cardiomyopathy was established to perform molecular biological and pathological assays on rat myocardium after intraperitoneal injection using AP39 and *in vitro* culture H9c2 cardiomyocytes for molecular biological assays after corresponding drug intervention. This study revealed the effects of mitochondria-targeted H_2S on mitophagy, the AMPK-ULK1-FUNDC1 pathway, and cardiomyocyte pyroptosis in doxorubicin-induced cardiomyopathy. This study provides new potential targets for antitumor drug-associated cardiomyopathy and myocardial fibrosis prevention and contributes to regulating mitochondrial physiological functions by H_2S.

RESULTS

AP39 promotes mitochondrial H_2S production in cardiomyocytes

The expression of CSE, a key enzyme for endogenous H_2S production, was examined using western blot and myocardial H_2S content detected by a H_2S assay kit to investigate the effect of AP39 in the production of H_2S in rat cardiomyocytes. The expression of CSE ($p = 0.0005$) (Figure 1A) and myocardial H_2S content (Figure 1C) was significantly decreased in the DOX group compared with the control group. Additionally, CSE ($p = 0.0003$) was significantly upregulated in the DOX+AP39 group compared with the DOX group after the AP39 intervention. At the same time, PAG blocked the upregulation of CSE ($p < 0.0001$) and myocardial H_2S content by AP39. Still, the difference between the control, AP39, and DMSO groups was insignificant.

A mitochondrial H_2S fluorescence probe was used to detect changes in mitochondrial H_2S production in H9c2 cardiomyocytes to further investigate the effect of AP39 on mitochondrial H_2S production in cardiomyocytes. The mitochondrial H_2S fluorescence signal was significantly weaker in the DOX group than in the control group, and the mitochondrial H_2S fluorescence signal was significantly enhanced in the DOX+AP39 group compared to the DOX group. In contrast, the DOX+AP39+PAG group showed a significant decrease in H_2S fluorescence signal compared to the DOX+AP39 group (Figure 1D). The expression of CSE in H9c2 cardiomyocytes was also detected using western blot. The CSE ($p < 0.0001$) protein expression was reduced in the DOX group compared to the control group. The CSE ($p < 0.0001$) protein expression was significantly upregulated in the DOX+AP39 group compared to the DOX group. PAG reversed the aforementioned changes in the DOX+AP39 group. In contrast, there was no significant statistical difference between the control, AP39, and DMSO groups. The aforementioned *in vivo* and *in vitro* experiments showed that DOX decreased mitochondrial H_2S production in cardiomyocytes. At the same time, AP39 increased mitochondrial H_2S production and upregulated CSE expression in cardiomyocytes.

AP39 ameliorates doxorubicin-induced myocardial fibrosis

Collagen- and fibrosis-related protein or RNA expression was detected using Masson staining, immunohistochemistry, real time quantitative polymerase chain reaction (RT-qPCR), and western blot to investigate the effect of AP39 on doxorubicin-induced myocardial fibrosis in rats. Compared to the control group, the DOX group showed disturbed myocardial fiber arrangement, structural disorders (Figure 2A), significantly increased myocardial collagen volume fraction ($p < 0.0001$) (Figures 2C and 2D), and significantly increased collagen III immunohistochemical-positive area ($p < 0.0001$) (Figures 2B–2E). In addition, it notably upregulated *Col2a1* mRNA expression ($p < 0.0001$) (Figure 2F) and significantly upregulated collagen III ($p < 0.0001$), α-SMA ($p = 0.0004$), MMP8 ($p < 0.0001$), MMP13 ($p < 0.0001$), and TIMP1 ($p = 0.0023$) protein expression (Figures 2G–2L).

In the DOX+AP39 group, compared to the DOX group, myocardial fiber structure was normal, myocardial fibers were more neatly arranged, collagen volume fraction was reduced ($p < 0.0001$), and collagen III immunohistochemistry-positive area ($p = 0.0097$) was

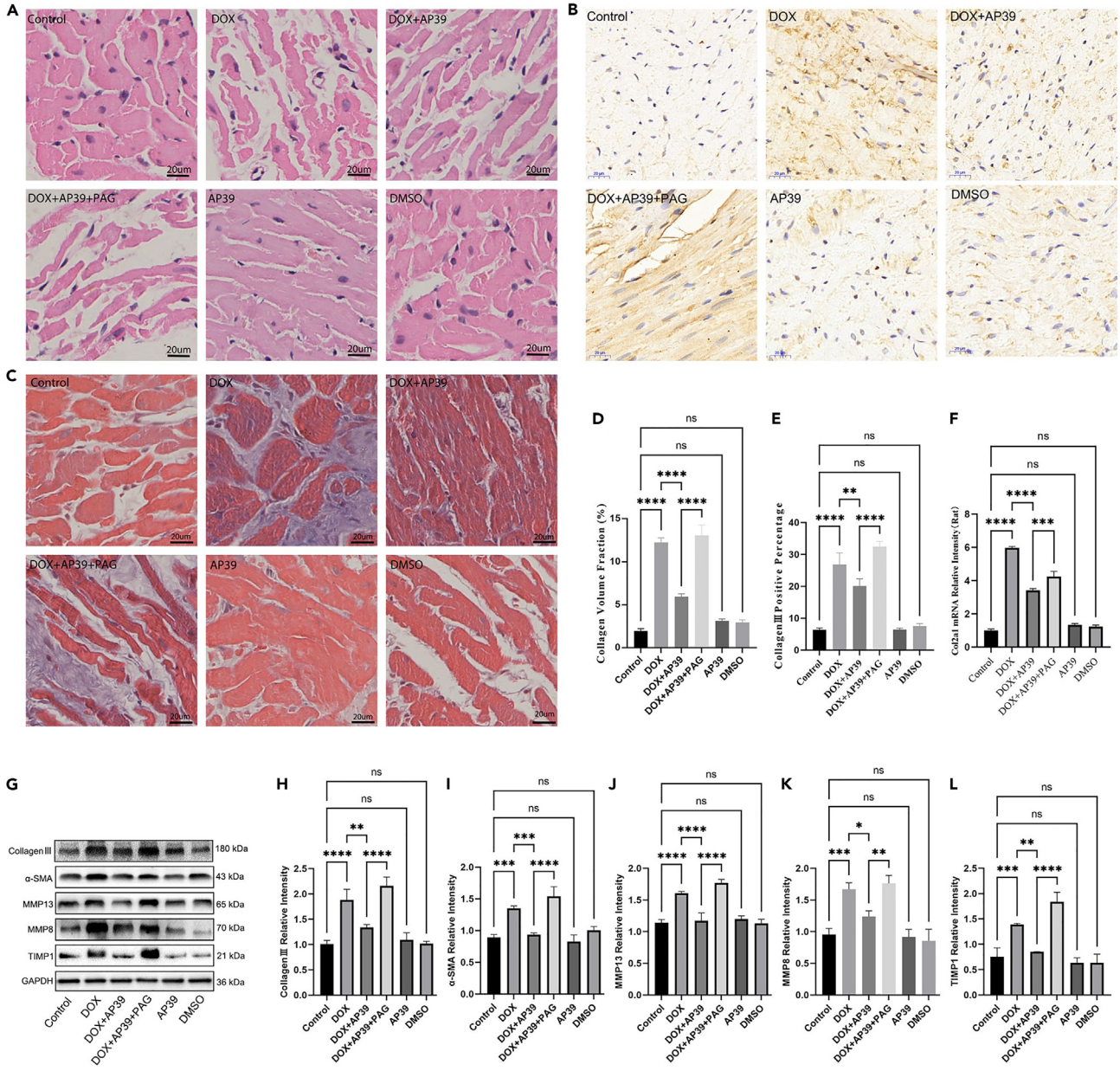

Figure 2. Effect of targeted mitochondrial H_2S on the structure and fibrosis of DOX-treated rat myocardial tissue

(A) HE staining of rat myocardial tissue, pink is the cytoplasm, blue part is the nucleus (Scale bar: 20 μm).

(B) Immunohistochemical staining results of collagen III of rat myocardial tissue, yellow part is collagen III positive (Scale bar: 20 μm).

(C) Masson staining of rat myocardial tissue, the blue part is collagen fiber (Scale bar: 20 μm).

(D) Calculated results of the collagen volume fraction of rat myocardial tissue in each group.

(E) Calculated results of collagen III immunohistochemistry of rat myocardial tissue in each group.

(F) Changes in the mRNA expression levels of *Col2a1*.

(G–L) Changes in collagen III, α-SMA, MMP13, MMP8, and TIMP1 protein expression levels in rat myocardial tissue and corresponding semiquantitative analysis results. Data were represented as mean ± SEM. *p < 0.05, **p < 0.01, ***p < 0.001, and ****p < 0.0001.

significantly reduced. In addition, the mRNA expression of *Col2a1* ($p < 0.0001$) was greatly downregulated, and the expression of collagen III ($p = 0.0029$), α-SMA ($p = 0.0004$), MMP8 ($p < 0.0001$), MMP13 ($p < 0.0001$), and TIMP1 ($p = 0.0023$) proteins was downregulated. In contrast, the DOX+AP39+PAG group reversed these changes in the DOX+AP39 group. The aforementioned results suggest that mitochondria-targeted H_2S ameliorates doxorubicin-induced myocardial fibrosis and reduces collagen synthesis and extracellular matrix deposition in rats.

Table 1. Ultrasound-related data for each group of rats

Group	Number	LVEDd (mm)	LVESd (mm)	LVFS (%)
Control	10	5.01 ± 0.42	2.42 ± 0.16	51.42 ± 4.38
DOX	7	5.63 ± 0.63*	3.27 ± 0.61*	39.94 ± 8.56*
DOX+AP39	8	4.96 ± 0.27#	2.51 ± 0.25#	50.69 ± 2.96#
DOX+AP39+PAG	7	5.42 ± 0.39	3.19 ± 0.41$	39.01 ± 5.10$
AP39	10	4.95 ± 0.31	2.56 ± 0.15	48.24 ± 2.02
DMSO	10	4.89 ± 0.35	2.50 ± 0.13	48.69 ± 2.30

LVEDd, left ventricular end-diastolic dimension; LVESd, left ventricular end-systolic diameter; LVFS, left ventricular fractional shortening.
*$p < 0.05$ vs. Control; #$p < 0.05$ vs. DOX; \$$p<0.05$ vs. DOX+AP39.

AP39 improves cardiac function and myocardial remodeling in rats with doxorubicin-induced cardiomyopathy

The structure and cardiac function of the heart were measured using color Doppler ultrasound to investigate the effect of AP39 on the function and structure of the heart in rats with doxorubicin-induced myocardial fibrosis. The heart weight (HW) and body weight (BW) of the rats were weighed, and HW/BW values were calculated.

The results showed that the left ventricular end-systolic diameter (LVESd) ($p < 0.0001$), left ventricular end-diastolic diameter (LVEDd) ($p = 0.0338$), and HW/BW values ($p < 0.0001$) were significantly increased. Left ventricular fractional shortening (LVFS) ($p < 0.0001$) values were significantly decreased in the DOX group compared to the control group. At the same time, LVESd ($p = 0.0003$), LVEDd ($p = 0.0276$) (Table 1; Figure 3), and HW/BW ($p = 0.0002$) values (Table 2) were significantly decreased, and LVFS ($p = 0.0004$) values increased in the DOX+AP39 group compared to the DOX group after the AP39 intervention.

Rats in the DOX+AP39+PAG group showed an increase in LVESd ($p = 0.0014$) and HW/BW ($p = 0.0009$) values and a decrease in LVFS ($p < 0.0001$) values compared to the DOX+AP39 group. The LVEDd ($p = 0.3063$) increased but was not statistically significant. At the same time, the differences between the control, AP39, and DMSO groups were not statistically significant. The aforementioned results suggest that doxorubicin may cause structural changes in the left ventricle and impair cardiac function. At the same time, AP39 may improve doxorubicin-induced impairment of cardiac function and alleviate the development of cardiac remodeling. PAG may interrupt the aforementioned protective effect of AP39 and worsen cardiac function, resulting in myocardial remodeling.

AP39 reduces doxorubicin-induced cardiomyocyte pyroptosis

Western blot was used to detect changes in the expression of propyroptosis proteins in H9c2 cardiomyocytes and to investigate the effect of AP39 on the pyroptosis of H9c2 cardiomyocytes after doxorubicin treatment. The expression of GSDMD-N ($p < 0.0001$), NLRP3 ($p < 0.0001$), cleaved-caspase1/caspase1 ($p < 0.0001$), and IL-1β ($p = 0.0006$) proteins was significantly increased in the DOX group compared with the control group (Figures 4D and 4I–4L). GSDMD-N ($p < 0.0001$), NLRP3 ($p < 0.0001$), cleaved-caspase1/caspase1 ($p < 0.0001$), and IL-1β ($p < 0.0001$) protein expression was significantly downregulated in the DOX+AP39 group compared with the DOX group. The DOX+AP39+PAG group reversed the aforementioned changes in the DOX+AP39 group, and the differences between the control, AP39, and DMSO groups were not statistically significant.

Western blot and RT-qPCR were used to explore the changes in the expression of pyroptosis-related markers in rat myocardial tissues in animal experiments and to investigate the effect of AP39 on the pyroptosis of doxorubicin-intervened rat cardiomyocytes. Compared with the control group, the expression of NLRP3 ($p = 0.0001$), GSDMD-N ($p = 0.0163$), cleaved-caspase1/caspase1 ($p = 0.0071$), and IL-1β ($p < 0.0001$) proteins was significantly upregulated (Figures 4C and 4E–4H). Additionally, the mRNA expression of *GSDMD* ($p < 0.0001$) and IL-1β ($p < 0.0001$) was significantly increased (Figures 4K and 4L) in the DOX group. The expression of NLRP3 ($p = 0.0001$), GSDMD-N ($p = 0.0062$), cleaved-caspase1/caspase1 ($p = 0.0003$), and IL-1β ($p = 0.0003$) was significantly downregulated. The mRNA expression of *GSDMD* ($p < 0.0001$) and *IL-1β* ($p < 0.0001$) was also significantly decreased (Figures 4A and 4B) in the DOX+AP39 group compared to the DOX group. PAG reversed the aforementioned changes in the DOX+AP39 group, and the differences between the control group and the AP39 and DMSO groups were not statistically significant. The aforementioned results suggest that cardiomyocyte pyroptosis was an important factor in doxorubicin-induced myocardial fibrosis, and AP39 could inhibit the development of doxorubicin-induced myocyte pyroptosis.

AP39 ameliorates mitochondrial dysfunction by upregulating FUNDC1-mediated mitophagy to inhibit doxorubicin-induced cardiomyocyte pyroptosis

Changes in mitophagy levels in H9c2 cardiomyocytes were detected using western blot to investigate the effect of mitophagy in H9c2 cardiomyocytes of AP39. Compared with the control group, LC3II/I ($p = 0.0002$), FUNDC1 ($p < 0.0001$), and beclin1 ($p < 0.0001$) protein expression was significantly downregulated, and P62 ($p < 0.0001$) was significantly upregulated in the DOX group (Figures 5A–5E). Compared with the DOX group, LC3II/I ($p < 0.0001$), FUNDC1 ($p = 0.0108$), and beclin1 ($p < 0.0001$) protein expression was significantly upregulated, and P62 ($p < 0.0001$) was significantly downregulated in the DOX+AP39 group. Compared with the DOX+AP39 group, FUNDC1-mediated mitophagy-related protein expression levels were significantly downregulated in the DOX+AP39+PAG group, with no significant statistical differences between the control, AP39, and DMSO groups.

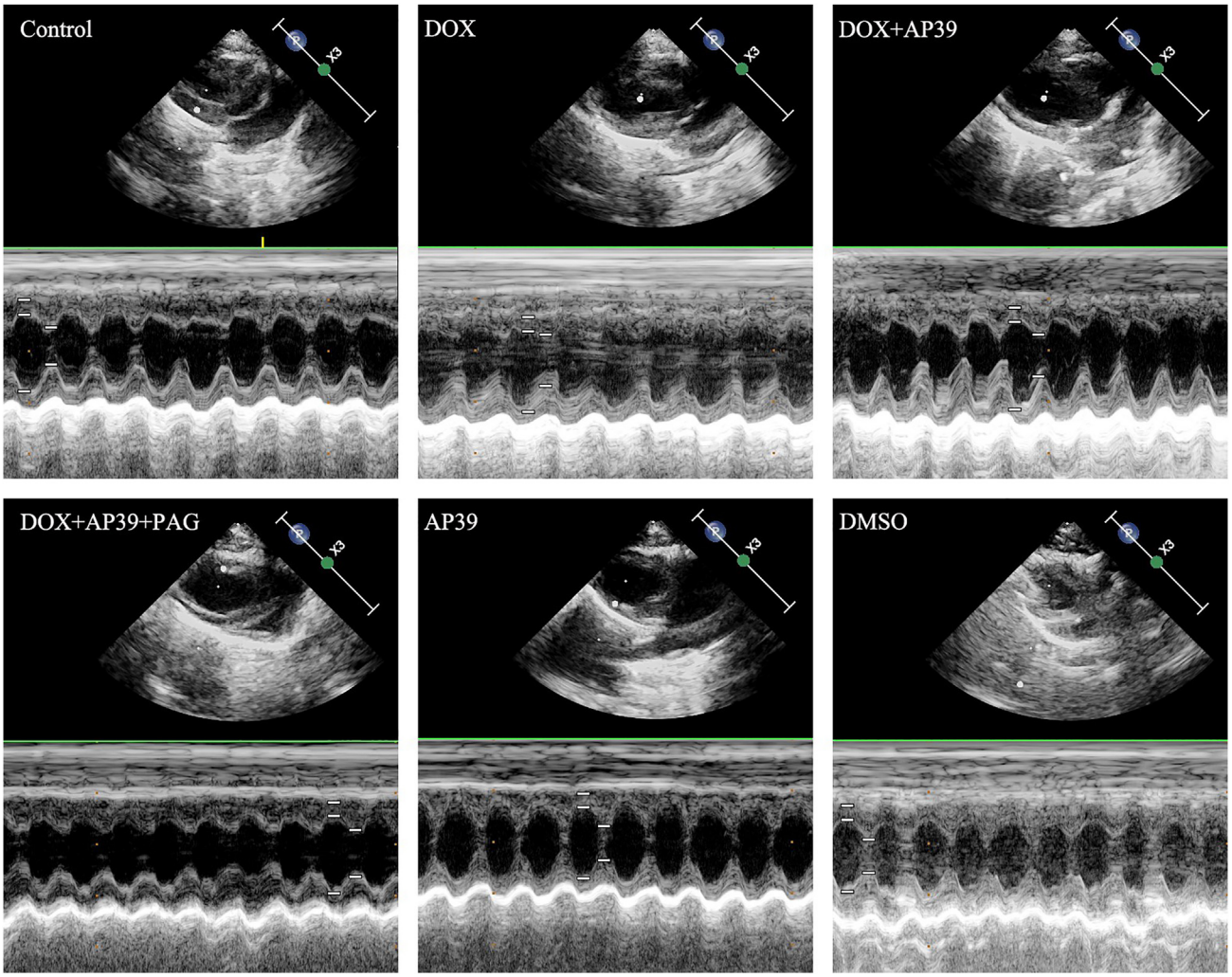

Figure 3. Effect of mitochondria-targeted H_2S on cardiac ultrasound in rats after DOX intervention
Groups: control, DOX, DOX+AP39, DOX+AP39+PAG, AP39, and DMSO.

The effect of AP39 on mitochondrial membrane potential and oxidative stress levels in H9c2 cardiomyocytes was explored using the JC1 mitochondrial membrane potential probe and the ROS probe. Compared with the control group, the green fluorescent signal of JC-1 increased, the red fluorescent signal decreased (Figure 5F), and the green fluorescent signal of ROS increased significantly in H9c2 cardiomyocytes in the DOX group (Figure 5F). Compared with the DOX group, the green fluorescence signal of JC-1 weakened, the red fluorescence signal increased, and the green fluorescence signal of ROS weakened in the DOX+AP39 group.

Transmission electron microscopy was used to observe microstructural changes in mitochondria and myocardial tissue to investigate the effect of AP39 on mitophagy in rat myocardium after doxorubicin intervention. Western blot and RT-qPCR were used to detect changes in mitophagy-related markers in rat cardiac tissue. Compared with the control group, the mitophagy phenomenon decreased significantly (Figure 6G). The expression of LC3II/I ($p = 0.0040$), beclin1 ($p = 0.0024$), and FUNDC1 ($p < 0.0001$) decreased, and that of P62 ($p < 0.0001$) protein and *P62* mRNA ($p < 0.0001$) increased significantly in the DOX group (Figures 6A–6F). LC3II/I ($p = 0.0056$), beclin1 ($p = 0.0025$), and FUNDC1 ($p = 0.0242$) expression was significantly increased, and P62 ($p = 0.0003$) protein and *P62* mRNA ($p < 0.0001$) expression was significantly decreased in the DOX+AP39 group compared with the DOX group. Meanwhile, the mitophagy phenomenon was significantly increased, but the changes in the DOX+AP39 group were reversed in the DOX+AP39+PAG group. There was no significant statistical difference between the control, AP39, and DMSO groups.

AP39 activates FUNDC1-mediated mitophagy via AMPK–ULK1 to ameliorate cardiomyocyte pyroptosis

The interaction among proteins was explored using STRING (https://cn.string-db.org/, Organisms: *Homo sapiens*) to investigate the effect of AP39 on the regulation of the AMPK–ULK1 pathway and FUNDC1-mediated mitophagy and cardiomyocyte pyroptosis. According to the

Table 2. Heart weight, body weight, and HW/BW value for each group of rats

Group	Number	BW (g)	HW (mg)	HW/BW
Control	10	254.70 ± 16.15	688.00 ± 45.14	2.71 ± 0.29
DOX	7	227.90 ± 9.81*	769.90 ± 111.80	3.37 ± 0.38*
DOX+AP39	8	244.50 ± 14.70#	678.80 ± 63.78	2.78 ± 0.18#
DOX+AP39+PAG	7	222.70 ± 1 0.92$	736.90 ± 67.62	3.31 ± 0.22$
AP39	10	255.50 ± 17.23	677.00 ± 43.69	2.65 ± 0.11
DMSO	10	250.10 ± 20.50	651.90 ± 48.79	2.61 ± 0.17

BW, body weight; HW, heart weight; HW/BW, heart weight/body weight.
*$p < 0.05$ vs. Control; #$p < 0.05$ vs. DOX; \$$p<0.05$ vs. DOX+AP39.

STRING database, there may be an interaction between ULK1 and FUNDC1. There may also be direct interactions among AMPK, ULK1, and FUNDC1 (Figure 7C). Therefore, a western blot was used to detect the protein expression of the AMPK-ULK1 pathway in animal experiments. The expression of P-AMPK/AMPK ($p < 0.0001$) and P-ULK1/ULK1 ($p = 0.0028$) was reduced in the myocardial of the DOX group compared with the control group (Figures 7A and 7D–7E). The expression of P-AMPK/AMPK ($p < 0.0001$) and P-ULK1/ULK1 ($p = 0.0011$) was significantly upregulated in the DOX+AP39 group compared with the DOX group. At the same time, PAG reversed the trend of AMPK–ULK1 pathway proteins in the DOX+AP39 group.

Similar changes were found in the *in vitro* experiments. Compared with the control group, the P-AMPK/AMPK ($p < 0.0001$) and P-ULK1/ULK1 ($p = 0.0028$) values of H9c2 cardiomyocytes in the DOX group were significantly decreased. In contrast, the P-AMPK/AMPK ($p < 0.0001$) and P-ULK1/ULK1 ($p = 0.0011$) values in the DOX+AP39 group were significantly increased in the DOX+AP39 group. Meanwhile, PAG could inhibit the aforementioned effects in the DOX+AP39 group. There was no statistically significant difference between the control, AP39, and DMSO groups (Figures 7B and 7F–7G).

We further revealed the relationship between AP39 and the AMPK-ULK1 pathway and FUNDC1-mediated mitophagy and pyroptosis. The AMPK inhibitor dorsomorphin and the ULK1 inhibitor SBI-0206965 were used in *in vitro* experiments to investigate whether AP39 could regulate FUNDC1-mediated mitophagy through the AMPK-ULK1 pathway and inhibit doxorubicin-induced cardiomyocyte pyroptosis. The expression of P-AMPK/AMPK (Dor: $p < 0.0001$; SBI-6965: $p < 0.0001$) and P-ULK1/ULK1 (Dor: $p = 0.0007$; SBI-6965: $p = 0.0001$) decreased significantly in the DOX+AP39+Dor (Figures 8C and 8D) and DOX+AP39+SBI-6965 groups (Figures 9C and 9D) compared with the DOX+AP39 group. FUNDC1-mediated mitophagy was suppressed. LC3II/I (Dor: $p < 0.0001$; SBI-6965: $p < 0.0001$), FUNDC1 (Dor: $p = 0.0003$; SBI-6965: $p = 0.0023$), and beclin1 (Dor: $p < 0.0001$; SBI-6965: $p < 0.0001$) proteins were significantly downregulated (Figures 8A and 8E–8H; Figures 9A and 9E–9H). In contrast, the expression of P62 (Dor: $p = 0.0391$; SBI-6965: $p = 0.0126$) protein was upregulated, and the expression of GSDMD-N (Dor: $p < 0.0001$; SBI-6965: $p = 0.0096$), cleaved-caspase1/caspase1 (Dor: $p < 0.0001$; SBI-6965: $p < 0.0001$), IL-1β (Dor: $p = 0.0037$; SBI-6965: $p < 0.0001$), and NLRP3 (Dor: $p < 0.0001$; SBI-6965: $p = 0.0004$) was significantly upregulated (Figure 8B and 8I–8L; Figure 9B and 9I–9L). These results suggest that mitochondria-targeted H_2S can regulate the AMPK-ULK1 pathway and FUNDC1-mediated mitophagy to inhibit cardiomyocyte pyroptosis.

DISCUSSION

H_2S is an important member of gaseous signaling molecules and has been found to have anti-myocardial fibrosis effects. Cardiotoxic effects caused by doxorubicin limit the prognosis of cancer patients. Mitochondria are the energy metabolism center of cells, and damaged mitochondria are an essential contributor to the cardiotoxicity of doxorubicin. Further investigation of the effect of the gas signaling molecule mitochondrial-targeted H_2S on FUNDC1-mediated mitophagy on cardiomyocyte pyroptosis is critical for understanding the molecular mechanisms of anthracycline-induced myocardial fibrosis and the cardiovascular physiological mechanisms of action of H_2S. Doxorubicin and mitochondria-targeted H_2S through *ex vivo* experiments in this study were administered to reveal the effects and molecular mechanisms of mitochondria-targeted H_2S on doxorubicin-induced myocardial fibrosis. Mitochondria-targeted H_2S reduced doxorubicin-induced collagen fiber synthesis and inhibited the expression of pyroptosis synthesis proteins in rats and H9c2 cardiomyocytes. It was accompanied by the upregulation of FUNDC1-associated mitophagy proteins, improved mitochondrial membrane potentials, and reduced ROS. This study will provide a new therapeutic strategy for the clinical intervention of anthracycline cardiotoxicity and a new theoretical basis for regulating doxorubicin-induced cardiomyopathy by mitochondria-targeted H_2S.

Myocardial fibrosis is a critical end-stage pathological change in a wide range of cardiovascular events, often leading to irreversible heart failure in the later stages of the disease and severely limiting the quality of life and long-term prognosis of patients.[23] Doxorubicin improves the 5-year survival rate of patients with malignant tumors. However, it is limited by its dose-dependent cardiotoxic effects, and myocardial fibrosis is the main pathological feature of doxorubicin-induced cardiomyopathy.[24] Therefore, suppressing the progression of fibrosis is crucial to improving the prognosis of patients with cardiovascular disease and the cardiotoxic effects of anti-cancer drugs.[25] Inhibition of myocardial fibrosis improves doxorubicin-induced cardiac injury and dysfunction.[26] In this study, doxorubicin significantly enhanced myocardial fibrosis, and the expression of collagen III, α-SMA, MMP3, MMP8, and TIMP1 proteins was upregulated in myocardial tissue.

Combined with cardiac ultrasound data and HW/BW values, the DOX group degraded cardiac function and remodeling, while mitochondria-targeted H_2S significantly improved doxorubicin-induced fibrosis and cardiac function. Meanwhile, our previously published results

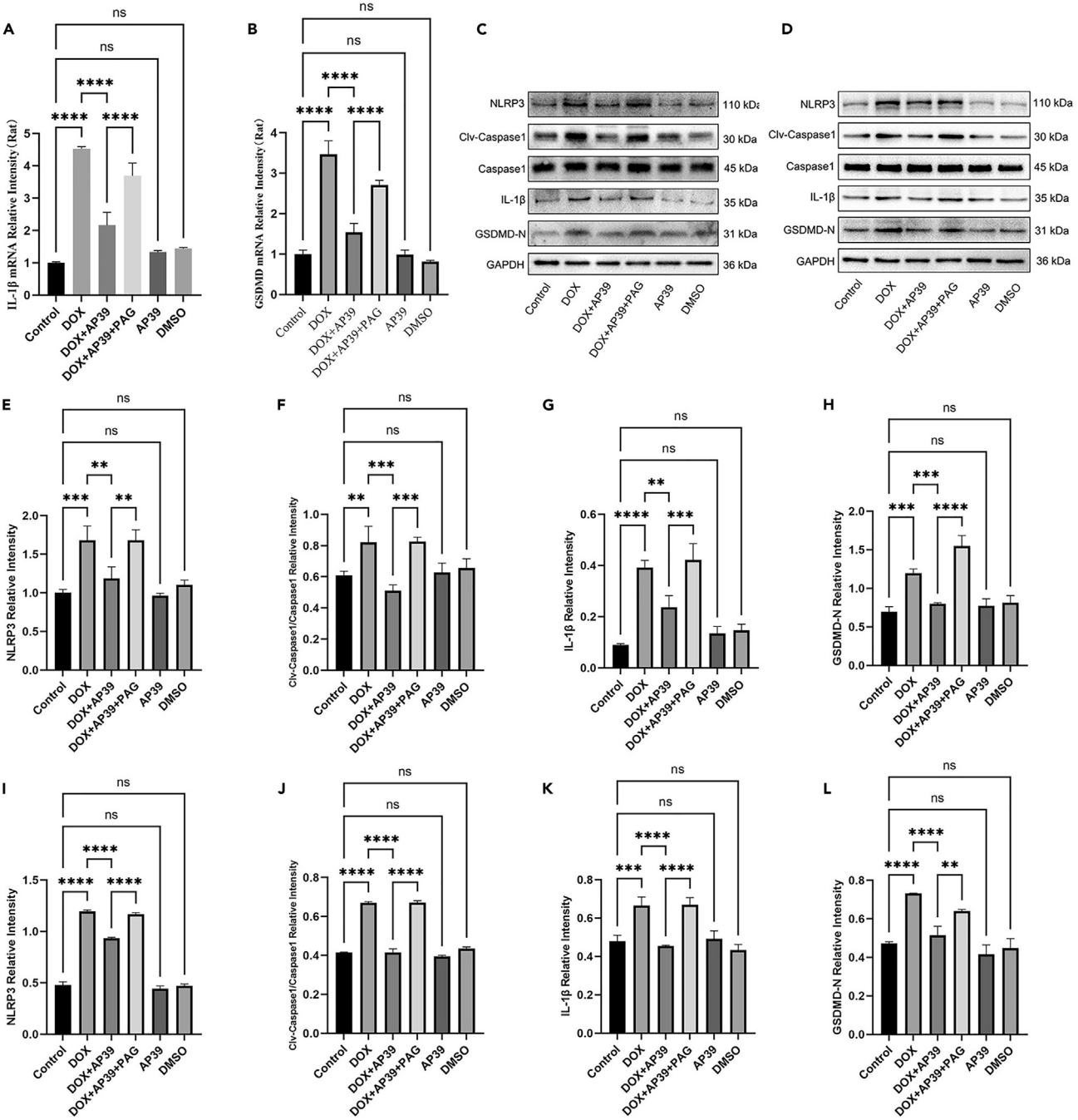

Figure 4. Effect of mitochondria-targeted H_2S on doxorubicin-induced cardiomyocyte pyroptosis

(A) Relative mRNA expression of IL-1β.

(B) Relative mRNA expression of GSDMD.

(C, E–H) Effect of AP39 on NLRP3, Clv-caspase1, caspase1, IL-1β, and GSDMD-N protein expression in rat myocardial tissue after doxorubicin intervention, and corresponding semiquantitative analysis.

(D, I–L) The effect of AP39 on NLRP3, Clv-caspase1, caspase1, IL-1β, and GSDMD-N protein expression in H9c2 cardiomyocytes after doxorubicin intervention. The above results were replicated independently three times. Data were represented as mean ± SEM. *$p < 0.05$, **$p < 0.01$, ***$p < 0.001$, and ****$p < 0.0001$.

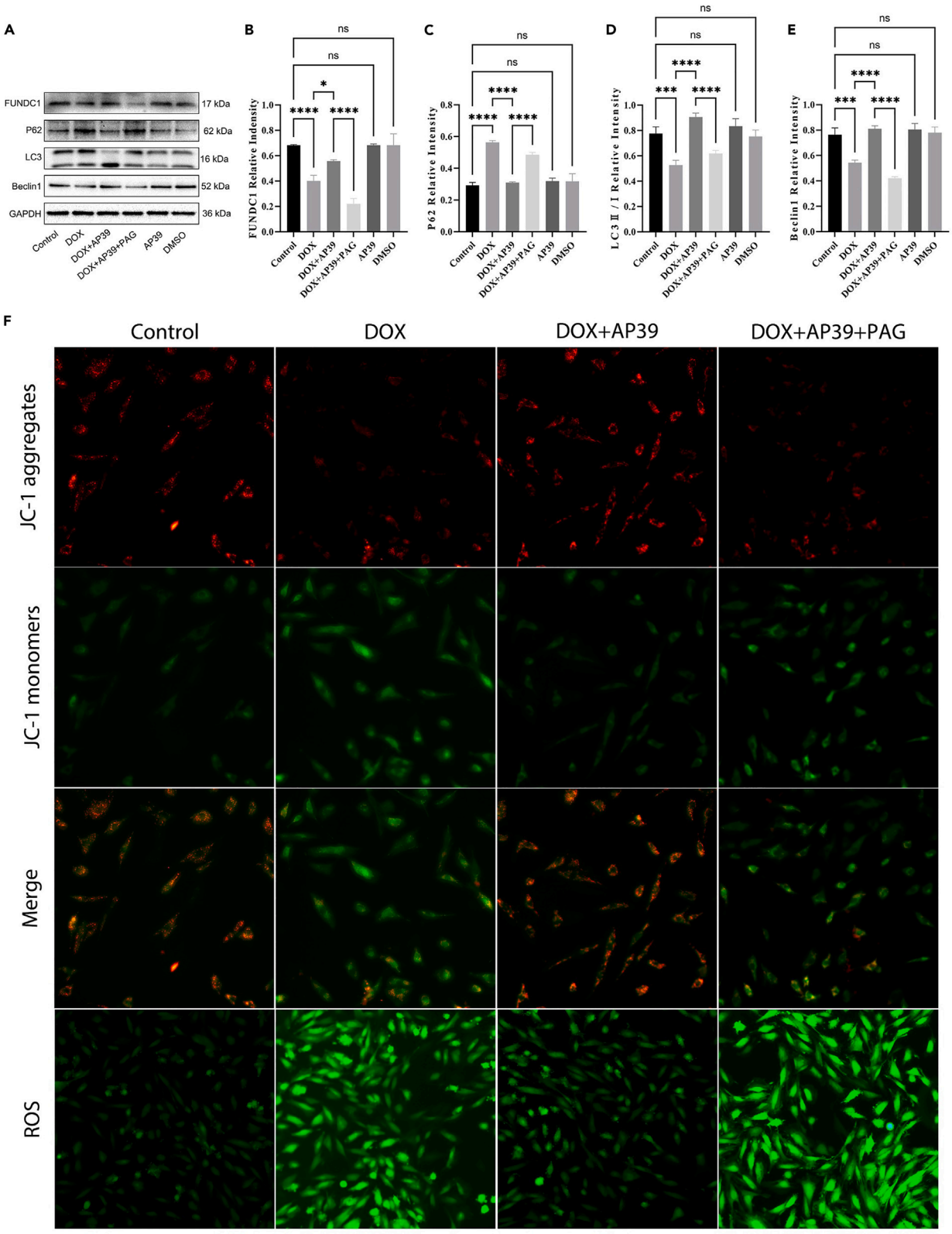
A
FUNDC1
P62
LC3
Beclin1
GAPDH
17 kDa
62 kDa
16 kDa
52 kDa
36 kDa
Control
DOX
DOX+AP39
DOX+AP39+PAG
AP39
DMSO
B
FUNDC1 Relative Indensity
C
P62 Relative Intensity
D
LC3 Ⅱ / Ⅰ Relative Intensity
E
Beclin1 Relative Intensity
ns
*
***
****
F
Control
DOX
DOX+AP39
DOX+AP39+PAG
JC-1 aggregates
JC-1 monomers
Merge
ROS

Figure 5. Effect of mitochondria-targeted H_2S on FUNDC1-mediated mitophagy, mitochondrial membrane potential, and ROS

(A–E) Effect of AP39 on FUNDC1, P62, LC3II/I, and beclin1 protein expression in H9c2 cardiomyocytes after DOX intervention and corresponding semiquantitative analysis.

(F) First to third line: Effect of AP39 with DOX intervention on H9c2 mitochondrial membrane potential. Red fluorescence indicates healthy mitochondrial membrane potential, and green fluorescence indicates reduced/impaired mitochondrial membrane potential. Fourth line: Effect of AP39 on ROS production in H9c2 cardiomyocytes after DOX intervention. Green fluorescence indicates ROS positivity. The above results were independently repeated three times. Data were represented as mean ± SEM. *$p < 0.05$, **$p < 0.01$, ***$p < 0.001$, and ****$p < 0.0001$.

showed that H_2S inhibited doxorubicin-induced myocardial fibrosis and cardiomyocyte apoptosis,[27] which is also consistent with the present study. The results of the present study found that doxorubicin could lead to cardiomyocyte damage and cardiac fibrotic repair, leading to cardiac remodeling and impaired cardiac function in rats, ultimately leading to a poor prognosis in patients treated with anthracycline chemotherapy. In contrast, mitochondria-targeted H_2S could improve myocardial remodeling and myocardial fibrosis induced by doxorubicin and reduce the cardiotoxic effects of doxorubicin. To some extent, mitochondria-targeted H_2S could preserve damaged cardiac heart function, and inhibiting pathological myocardial remodeling minimizes the incidence of myocardial fibrosis.

Cell pyroptosis can be induced by recruiting NLRP3 inflammatory vesicles and activating caspase1 to activate inflammatory factors, such as IL-1β, after cell injury. After that, the cleavage of GSDMD proteins causes the formation of cell membrane pore channels. Recent studies have found that cardiomyocyte pyroptosis is an essential contributor to the development of cardiomyopathy, and that NLRP3/caspase1-mediated cardiomyocyte pyroptosis promotes the development of myocardial fibrosis.[28] In doxorubicin-induced myocardial damage and myocardial fibrosis, doxorubicin could induce pyroptosis and promote myocardial fibrosis and myocardial remodeling, leading to the deterioration of cardiac function.[29,30] In this study, doxorubicin caused a significant increase in the expression of NLRP3, GSDMD-N, cleaved-caspase1/caspase1, and IL-1β. *In vitro* studies have also found that doxorubicin increased the expression of H9c2 cardiomyocyte pyroptosis-related proteins.

Doxorubicin was found to bind directly to GSDMD and to promote GSDMD-N-mediated cardiomyocyte pyroptosis. This process directly affects damaged mitochondria and cardiomyocytes, possibly the primary mechanism of doxorubicin-induced cardiotoxicity and cardiomyopathy.[31] The aforementioned findings suggest that doxorubicin inhibits and kills tumor cells while also causing a toxic response and toxic effect on cardiomyocytes, and that inflammatory response-related cardiomyocyte pyroptosis may be an important factor in cardiotoxicity during doxorubicin use. Cardiocyte pyroptosis may be an essential target for intervention in antitumor drug-associated cardiomyopathy.

Mitophagy is an essential cellular physiological activity in response to stress or injury by degrading damaged mitochondria to remove excess metabolic waste and using the absorbed mitochondria as raw materials for cellular synthesis and metabolism. Defective mitophagy has been shown to lead to the development of cardiomyopathy and myocardial fibrosis,[12,32] and FUNDC1 is a vital regulator of mitophagy and mitochondrial dynamics.[33] Defective mitophagy is also an important factor in the cardiotoxicity and myocardial injury of doxorubicin, and preserving impaired mitophagy alleviates doxorubicin-induced cardiac dysfunction.[34,35] The imbalance of mitophagy will lead to mitochondrial damage or failure to remove toxins promptly, accumulation of harmful metabolites, increased production of reactive oxygen species, and mitochondrial dysfunction, finally leading to cellular pyroptosis.[36,37] However, the role of FUNDC1-mediated mitophagy and pyroptosis in the development of cardiomyopathy has not been elucidated. This study found a decreased ratio of mitophagy markers, such as FUNDC1, LC3II/I, and beclin1, due to the decrease of LC3II produced by ubiquitination of LC3I. Autophagy substrate P62 accumulation was found after doxorubicin intervention.

To some extent, LC3II/I indicated the degree of LC3 activity. Doxorubicin induced a decrease in FUNDC1-mediated mitophagy. In addition, it also caused a reduction in mitochondrial membrane potential and an accumulation in oxidative stress, along with a significant increase in the expression of pyroptosis formation proteins. In contrast, mitochondria-targeted H_2S increased FUNDC1-mediated mitophagy, alleviated the decrease in mitochondrial membrane potential, reduced oxidative stress, and decreased pyroptosis protein expression in cardiomyocytes. These results suggest that impaired FUNDC1-mediated mitophagy is a vital mechanism for the cardiotoxic effects of doxorubicin. These results also suggest that mitochondrial-targeted H_2S can upregulate FUNDC1-mediated mitophagy, preserve mitochondrial function, restore impaired mitochondrial membrane potential, reduce oxidative stress, and reduce cardiomyocyte pyroptosis.

The AMPK-ULK1 pathway is a crucial pathway for autophagy regulation. AMPK can directly activate ULK1, induce the formation of ATG complexes and autophagosomes downstream of autophagy, regulate autophagy in response to energy changes and nutrient signaling, and activate the AMPK-ULK1 signaling pathway-mediated autophagy, inhibiting the development of myocardial fibrosis.[38,39] Chen et al.[40] found that AMPK-ULK1-mediated protective autophagy reduced doxorubicin-induced myocardial injury and alleviated myocardial fibrosis while reducing cardiomyocyte apoptosis. In this study, doxorubicin caused a decrease in AMPK and ULK1 protein phosphorylation in rat myocardial tissue and H9c2 cardiomyocytes, accompanied by a reduction in FUNDC1-mediated mitophagy protein expression. However, the role of the AMPK-ULK1 pathway and FUNDC1-mediated mitophagy in doxorubicin-induced cardiomyopathy remains unclear. This study identified a direct interaction between ULK1 and FUNDC1 in the STRING protein interaction database. The subsequent addition of AMPK, a ULK1 inhibitor, to the study revealed that the corresponding downstream protein expression levels decreased with the inhibition of AMPK-ULK1-FUNDC1 pathway protein expression. This was accompanied by a decrease in mitophagy protein expression levels and an increase in pyroptosis protein expression.

Additionally, ULK1 was found to regulate mitochondrial function and inhibit cellular pyroptosis, and ULK1-ubiquitinated degradation, or ULK1 deficiency, impaired mitochondrial ROS clarity and induced cellular inflammatory vesicle-dependent cellular pyroptosis.[41] In contrast, Cai et al.[42] found that the AMPK-ULK1-FUNDC1 axis-mediated mitophagy preserved mitochondrial function and normalized mitochondrial fusion and division, thereby reducing myocardial ischemia-reperfusion injury. All of these studies support the results of the present study and

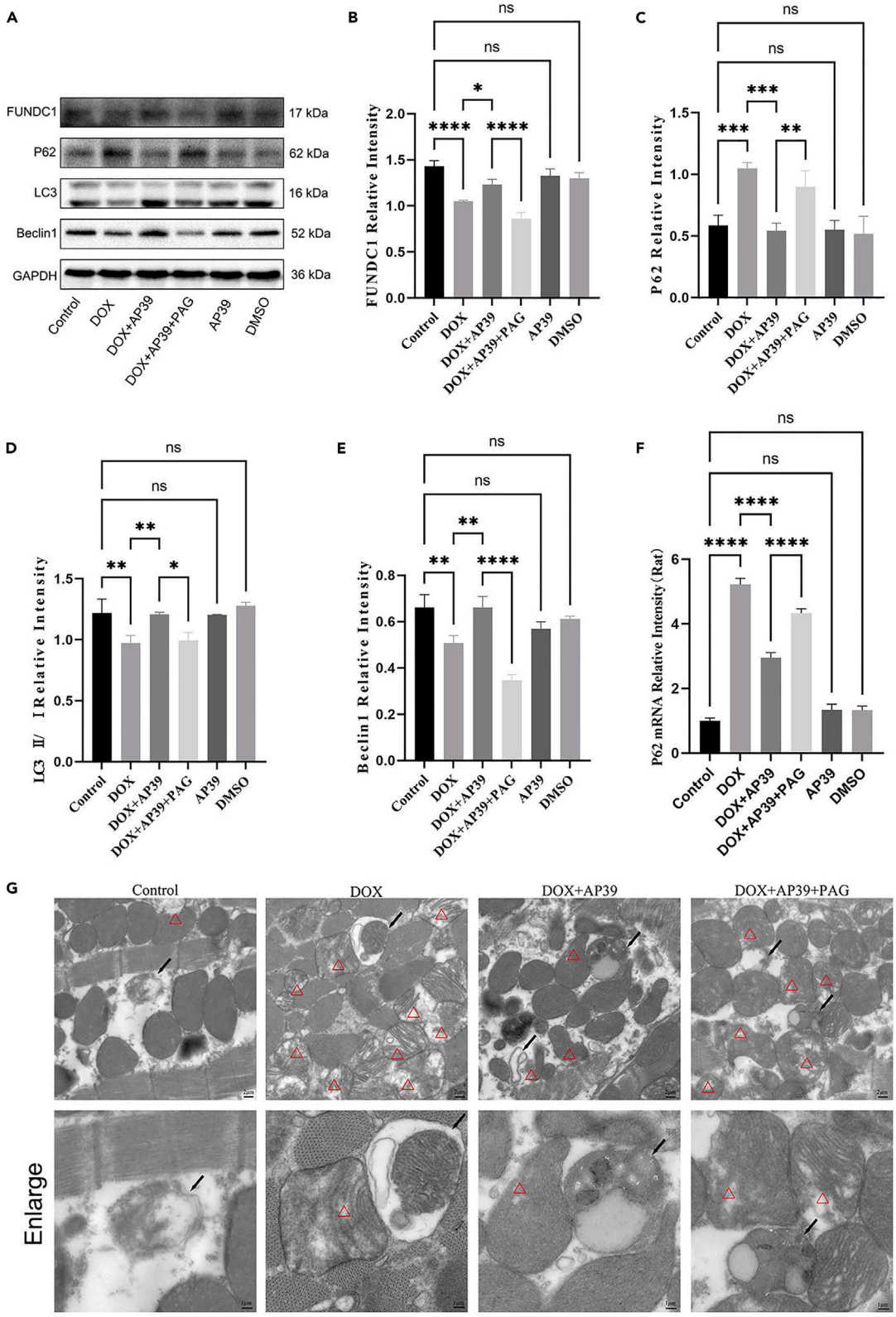
A
FUNDC1
P62
LC3
Beclin1
GAPDH
17 kDa
62 kDa
16 kDa
52 kDa
36 kDa
Control
DOX
DOX+AP39
DOX+AP39+PAG
AP39
DMSO
B
FUNDC1 Relative Intensity
C
P62 Relative Intensity
D
LC3 II/ I Relative Intensity
E
Beclin1 Relative Intensity
F
P62 mRNA Relative Intensity (Rat)
ns
G
Control
DOX
DOX+AP39
DOX+AP39+PAG
Enlarge

Figure 6. Effect of mitochondria-targeted H_2S on mitophagy in rat myocardial tissue after DOX intervention

(A–E) Effect of AP39 on FUNDC1, P62, LC3II/I, and beclin1 protein expression in rat myocardial after DOX intervention and corresponding semiquantitative analysis.

(F) Relative mRNA expression of *P62*. The above results were independently repeated three times.

(G) Transmission electron microscopy observation of microstructural changes in rat myocardial tissue. The "△" shows severely damaged mitochondria. The part indicated by the black arrow is mitophagy (Scale bar: 2 μm, enlarge: 1 μm). Data were represented as mean ± SEM. *p < 0.05, **p < 0.01, ***p < 0.001, and ****p < 0.0001.

further suggest that AMPK-ULK1-FUNDC1, a novel mitophagy regulatory pathway, may inhibit the myocardial pyroptosis process and may be a new target for antineoplastic drug-associated cardiomyopathy.

In recent years, H_2S has been a newly discovered third gas-signaling molecule. Since CSE, a key enzyme for H_2S production, is widely expressed in the heart, it may be an essential endogenous regulator of the cardiovascular system. In the present study, doxorubicin caused a decrease in H_2S content and impaired CSE production in rat myocardial tissues. Doxorubicin also reduced mitochondrial H_2S levels and endogenous H_2S synthesis in H9c2 cardiomyocytes. In contrast, mitochondria-targeted H_2S could somewhat alleviate the dysfunctional CSE synthesis induced by doxorubicin and target the enhancement of mitochondrial H_2S production in H9c2 cardiomyocytes. H_2S can antagonize the production of collagen fibers and the extracellular matrix in myocardial tissue and suppress the development of myocardial fibrosis.[43] Our previously published study also showed that H_2S could inhibit doxorubicin-induced myocardial fibrosis in rats, but the exact mechanism is unclear.[44] This study found that mitochondria-targeted H_2S inhibited doxorubicin-induced myocardial fibrosis and reduced collagen synthesis and extracellular matrix deposition, similar to our previous study.[27]

Further studies found that mitochondria-targeted H_2S reduced the occurrence of doxorubicin-induced myocardial cell pyroptosis, reduced cell necrosis and myocardial injury, and improved cardiac function to some extent. Kar et al.[45] also found that H_2S inhibited the occurrence of myocardial cell pyroptosis, improved cardiac function, and inhibited myocardial remodeling and cardiomyopathy. Mitochondria-targeted H_2S

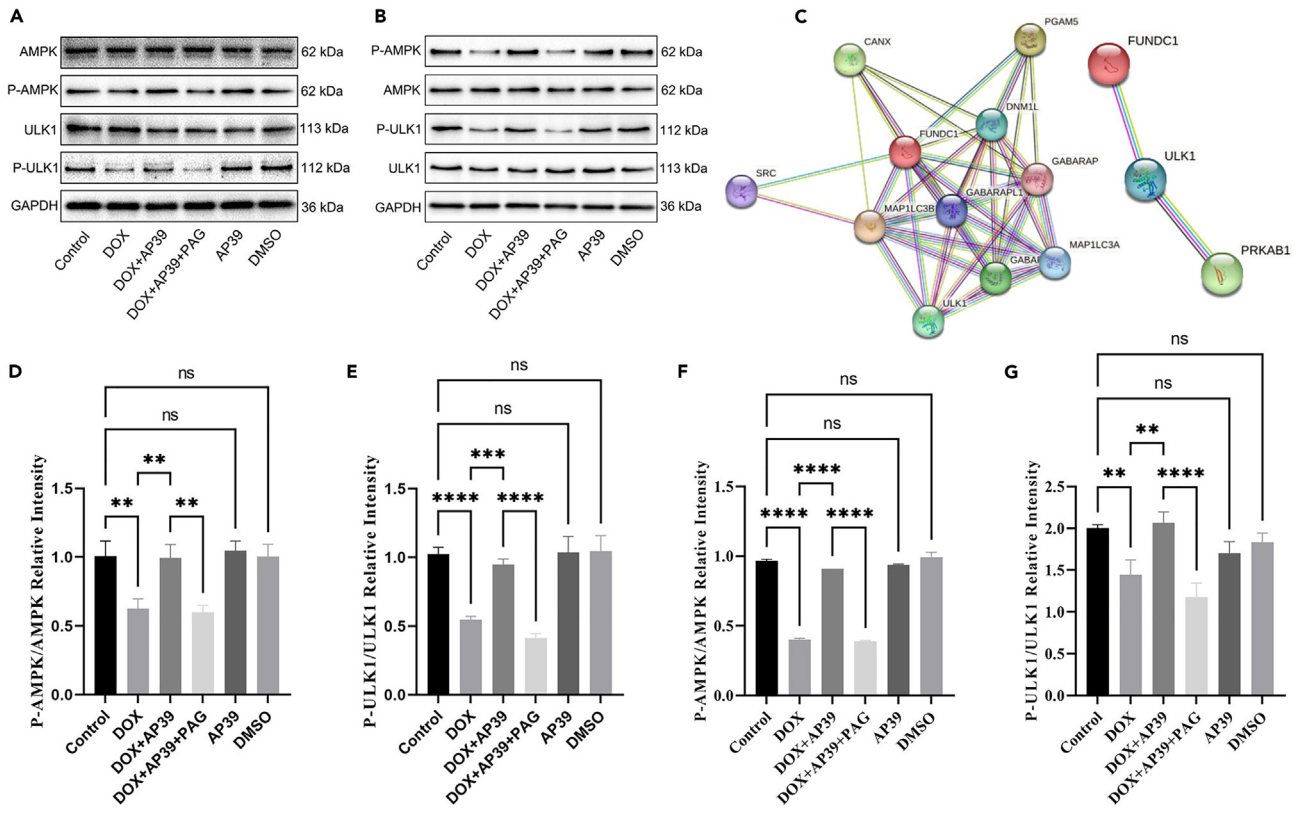

Figure 7. Effect of mitochondria-targeted hydrogen sulfide on the AMPK-ULK1-FUNDC1 pathway

(A, D, and E) Effect of AP39 on protein expression levels of AMPK, P-AMPK, ULK1, and P-ULK1 in rats myocardial, and the corresponding semiquantitative analysis of P-ULK1/ULK1 and P-AMPK/AMPK.

(B, F, and G) Effect of AP39 on protein expression levels of AMPK, P-AMPK, ULK1, and P-ULK1 in the H9c2 cell line, and the corresponding semiquantitative analysis of P-ULK1/ULK1 and P-AMPK/AMPK. C: Analysis of interactions among ULK1, FUNDC1, and AMPK in the STRING database. The above results were replicated independently three times. Data were represented as mean ± SEM. *p < 0.05, **p < 0.01, ***p < 0.001, and ****p < 0.0001.

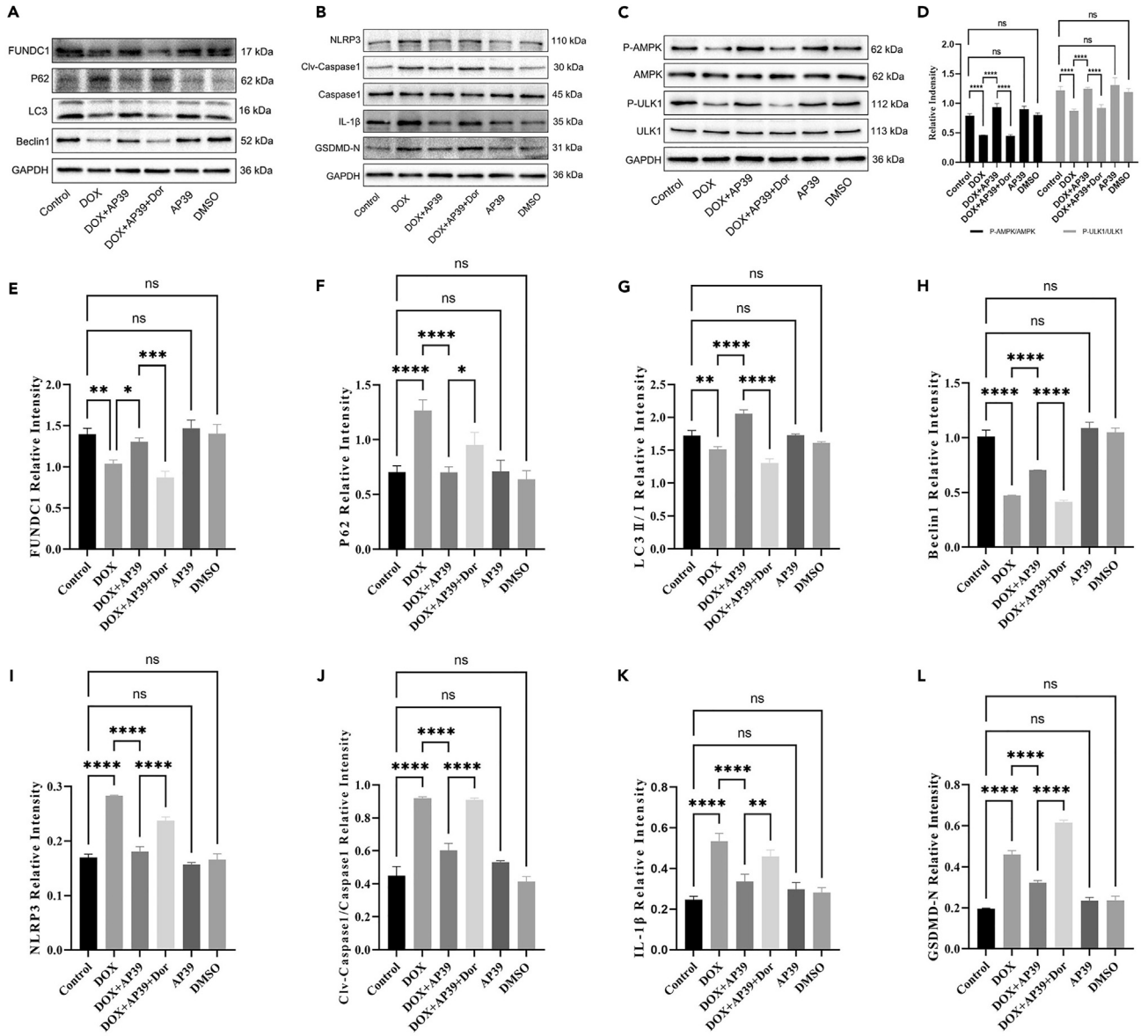

Figure 8. Effect of AMPK inhibitor (dorsomorphin) on AMPK-ULK1-FUNDC1 pathway-mediated mitophagy and pyroptosis in H9c2 cardiomyocytes

(A, E–H) Effect of AP39 and dorsomorphin on FUNDC1, P62, LC3II/I, beclin1 protein expression levels, and the corresponding semiquantitative analysis.

(B, I–L) Effect of AP39 and dorsomorphin on the expression levels of NLRP3, Clv-caspase1, caspase1, IL-1β, GSDMD-N, and the corresponding semiquantitative analysis.

(C, D) Effect of AP39 and dorsomorphin on protein expression levels of AMPK, P-AMPK, ULK1, P-ULK1, and the corresponding semiquantitative analysis of P-ULK1/ULK1 and P-AMPK/AMPK. The above results were replicated independently three times. Data were represented as mean ± SEM. *$p < 0.05$, **$p < 0.01$, ***$p < 0.001$, and ****$p < 0.0001$.

upregulated AMPK1-ULK1-FUNDC1-mediated mitophagy and alleviated the reduction of mitochondrial membrane potential in H9c2 cardiomyocytes while reducing ROS generation, thus inhibiting the occurrence of cardiomyocyte pyroptosis. The modulation of the AMPK1-ULK1-FUNDC1 pathway by mitochondria-targeted H_2S has not been reported in the present study after treatment with dorsomorphin (AMPK inhibitor), SBI-0206965 (ULK1 inhibitor), along with the administration of mitochondrial-targeted H_2S. In contrast, the downregulation of the expression levels of signaling pathways downstream of the AMPK-ULK1-FUNDC1 pathway and decreased FUNDC1-mediated mitophagy levels were observed, while cell pyroptosis increased.

Additionally, PAG (an endogenous H_2S-producing enzyme inhibitor) administration along with mitochondrial-targeted H_2S inhibited AMPK1-ULK1-FUNDC1 pathway-mediated mitophagy levels, leading to increased expression of pyroptosis in animal experiments and increasing doxorubicin-induced myocardial fibrosis. H_2S has been shown to promote mitophagy, reduce mitochondrial fragmentation

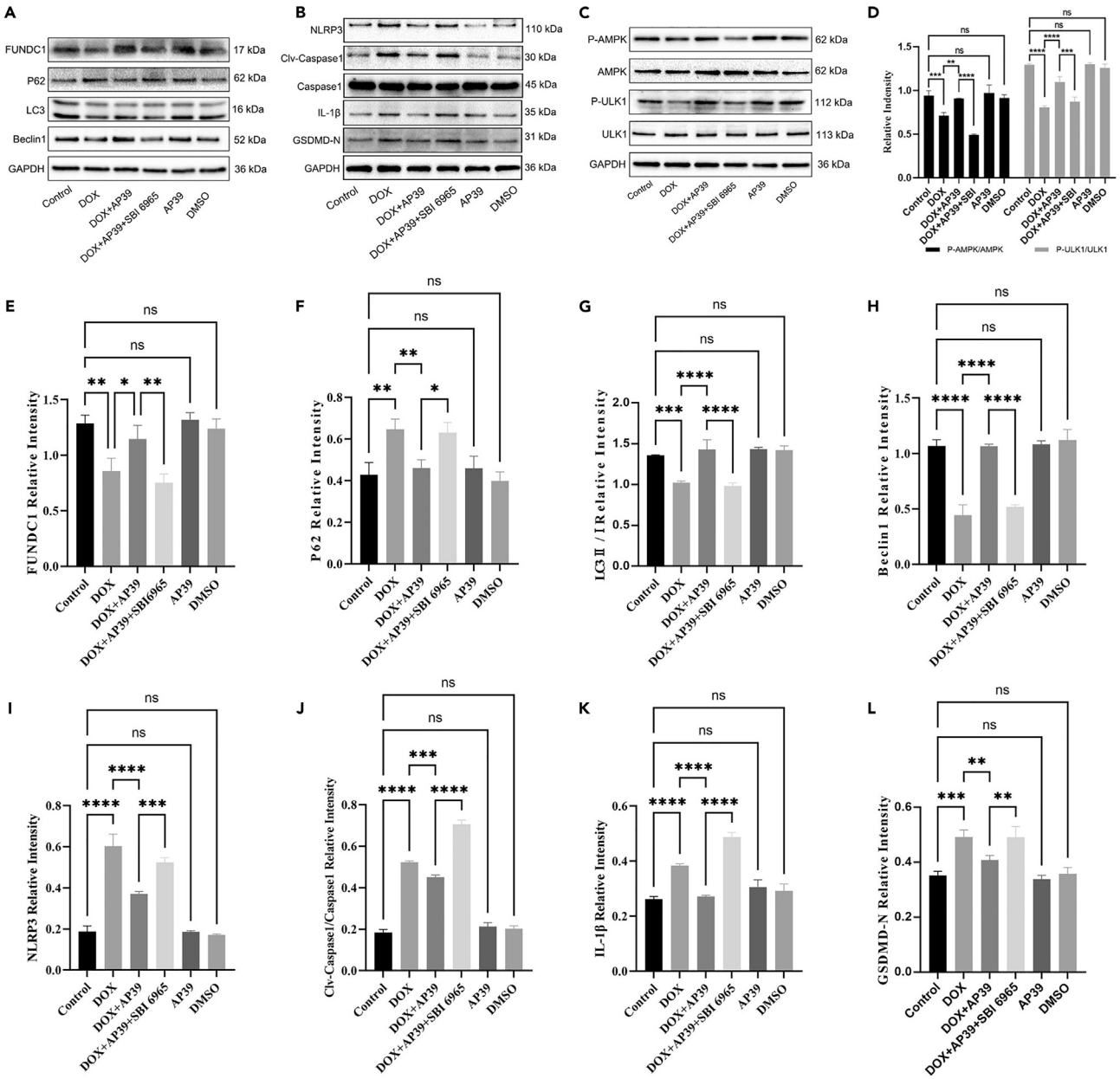

Figure 9. Effect of ULK1 inhibitor (SBI-0206965) on AMPK-ULK1-FUNDC1 pathway-mediated mitophagy and pyroptosis in H9c2 cardiomyocytes

(A, E–H) Effects of AP39 and SBI-0206965 on the expression levels of FUNDC1, P62, LC3II/I, beclin1 proteins, and the corresponding semiquantitative analysis.

(B, I–L) Effects of AP39 and SBI-0206965 on NLRP3, Clv-caspase1, caspase1, IL-1β, GSDMD-N protein expression levels, and the corresponding semiquantitative analysis.

(C, D) Effect of AP39 and SBI-0206965 on AMPK, P-AMPK, ULK1, and P-ULK1 protein expression levels, and the corresponding semiquantitative analysis of P-ULK1/ULK1 and P-AMPK/AMPK. The above results were replicated independently three times. Data were represented as mean ± SEM. *$p < 0.05$, **$p < 0.01$, ***$p < 0.001$, and ****$p < 0.0001$.

and ROS generation, and enhance mitochondrial respiratory chain activity, thereby facilitating myocardial injury.[46,47] Furthermore, impaired H_2S production leads to defective ULK1-dependent autophagy activation,[48] all of which correspond to our findings. These findings suggest that mitochondria-targeted H_2S could regulate AMPK1-ULK1-FUNDC1 pathway-mediated mitophagy levels, alleviate doxorubicin-induced dysfunctional mitochondrial membrane potential and ROS production, and inhibit cardiomyocyte pyroptosis. Additionally, mitochondria-targeted H_2S may be an essential target for mitochondria-targeted H_2S to ameliorate doxorubicin-induced myocardial fibrosis.

Conclusion

Our results suggest that defective AMPK1-ULK1-FUNDC1 pathway-mediated mitophagy could lead to mitochondrial dysfunction and cause cardiomyocyte pyroptosis. This process may be one of the essential mechanisms of doxorubicin-induced myocardial fibrosis and cardiotoxic effects. Mitochondria-targeted H_2S could increase mitochondrial H_2S production, upregulate AMPK-ULK1-FUNDC1-mediated mitophagy, inhibit cardiomyocyte pyroptosis and myocardial fibrosis, and improve mitochondrial and cardiac functions and myocardial remodeling. This study will provide new targets and strategies for preventing and treating the cardiotoxicity of antineoplastic anthracycline drugs and further reveal the intrinsic mechanism of antagonism of myocardial fibrosis by targeted gas signaling molecules.

Limitations of the study

However, this study still has many shortcomings. For instance, the small sample amount and experimental repetitions lack further exploration of the process of mitochondrial-targeted H_2S activation of FUNDC1-mediated mitophagy. In future works, we will increase the sample amount and experimental repetitions to further explore such issues.

STAR★METHODS

Detailed methods are provided in the online version of this paper and include the following:

- KEY RESOURCES TABLE
- RESOURCE AVAILABILITY
  - Lead contact
  - Materials availability
  - Date and code availability
- EXPERIMENTAL MODEL AND STUDY PARTICIPANT DETAILS
  - Animal experiments
  - *In vitro* studies
- METHOD DETAILS
  - Animal
  - Echocardiography
  - HW/BW
  - Masson staining
  - HE staining
  - Immunohistochemical staining
  - Transmission electron microscopy
  - Construction of the protein–protein interaction (PPI) network
  - Myocardial H_2S content testing
  - Cell culture
  - RT-qPCR
  - Mito-HS mitochondrial H_2S fluorescent probe assay
  - Mitochondrial membrane potential detection
  - Cellular reactive oxygen species detection
  - Western blot
- QUANTIFICATION AND STATISTICAL ANALYSIS
  - Statistical analysis

ACKNOWLEDGMENTS

This project was supported by the National Natural Science Foundation of China (No.82074236), Clinical Major Projects of Hunan Provincial Health Commission (No. 20201913), the Natural Science Foundation of Hunan Province (No.2021JJ70035, No. 2021JJ40499, and No. 2020JJ5505).

Thanks to Figdraw (www.figdraw.com, patent ID:PPUPP1aaa4) for supporting this experiment.

AUTHOR CONTRIBUTIONS

J.Z., T.Y., and J. Yi: investigation, data curation, software, formal analysis, resources, and methodology. H.H., Q.L., L.N., and M.L.: resources, validation, and investigation. C.C. and J. Yang: conceptualization, resources, data curation, software, formal analysis, supervision, funding acquisition, validation, investigation, visualization, methodology, writing – original draft, project administration, and writing – review and editing.

DECLARATION OF INTERESTS

The authors declare no conflicts of interest.

Received: August 8, 2023
Revised: January 10, 2024
Accepted: February 20, 2024
Published: February 23, 2024

REFERENCES

1. Xia, Y., Jin, J., Chen, A., Lu, D., Che, X., Ma, J., Li, S., Yin, M., Yang, Z., Lu, H., et al. (2023). Mitochondrial aspartate/glutamate carrier AGC1 regulates cardiac function via Drp1-mediated mitochondrial fission in doxorubicin-induced cardiomyopathy. Transl. Res. *261*, 28–40. https://doi.org/10.1016/j.trsl.2023.06.004.
2. Yang, M., Abudureyimu, M., Wang, X., Zhou, Y., Zhang, Y., and Ren, J. (2023). PHB2 ameliorates Doxorubicin-induced cardiomyopathy through interaction with NDUFV2 and restoration of mitochondrial complex I function. Redox Biol. *65*, 102812. https://doi.org/10.1016/j.redox.2023.102812.
3. Zhang, P., Lu, H., Wu, Y., Lu, D., Li, C., Yang, X., Chen, Z., Qian, J., and Ge, J. (2023). COX5A Alleviates Doxorubicin-Induced Cardiotoxicity by Suppressing Oxidative Stress, Mitochondrial Dysfunction and Cardiomyocyte Apoptosis. Int. J. Mol. Sci. *24*, 10400. https://doi.org/10.3390/ijms241210400.
4. You, J., Li, X., Dai, F., Liu, J., Zhang, Q., and Guo, W. (2023). GSDMD-mediated pyroptosis promotes cardiac remodeling in pressure overload. Clin. Exp. Hypertens. *45*, 2189138. https://doi.org/10.1080/10641963.2023.2189138.
5. Zhang, W., Wang, X., Tang, Y., and Huang, C. (2023). Melatonin alleviates doxorubicin-induced cardiotoxicity via inhibiting oxidative stress, pyroptosis and apoptosis by activating Sirt1/Nrf2 pathway. Biomed. Pharmacother. *162*, 114591. https://doi.org/10.1016/j.biopha.2023.114591.
6. Tan, Y., Zhang, Y., He, J., Wu, F., Wu, D., Shi, N., Liu, W., Li, Z., Liu, W., Zhou, H., and Chen, W. (2022). Dual specificity phosphatase 1 attenuates inflammation-induced cardiomyopathy by improving mitophagy and mitochondrial metabolism. Mol. Metab. *64*, 101567. https://doi.org/10.1016/j.molmet.2022.101567.
7. Li, W., Wang, X., Liu, T., Zhang, Q., Cao, J., Jiang, Y., Sun, Q., Li, C., Wang, W., and Wang, Y. (2022). Harpagoside Protects Against Doxorubicin-Induced Cardiotoxicity via P53-Parkin-Mediated Mitophagy. Front. Cell Dev. Biol. *10*, 813370. https://doi.org/10.3389/fcell.2022.813370.
8. Wang, S.-H., Zhu, X.-L., Wang, F., Chen, S.-X., Chen, Z.-T., Qiu, Q., Liu, W.-H., Wu, M.-X., Deng, B.-Q., Xie, Y., et al. (2021). LncRNA H19 governs mitophagy and restores mitochondrial respiration in the heart through Pink1/Parkin signaling during obesity. Cell Death Dis. *12*, 557. https://doi.org/10.1038/s41419-021-03821-6.
9. Jin, Q., Li, R., Hu, N., Xin, T., Zhu, P., Hu, S., Ma, S., Zhu, H., Ren, J., and Zhou, H. (2018). DUSP1 alleviates cardiac ischemia/reperfusion injury by suppressing the Mff-required mitochondrial fission and Bnip3-related mitophagy via the JNK pathways. Redox Biol. *14*, 576–587. https://doi.org/10.1016/j.redox.2017.11.004.
10. Zhang, Y., Wang, Y., Xu, J., Tian, F., Hu, S., Chen, Y., and Fu, Z. (2019). Melatonin attenuates myocardial ischemia-reperfusion injury via improving mitochondrial fusion/mitophagy and activating the AMPK-OPA1 signaling pathways. J. Pineal Res. *66*, e12542. https://doi.org/10.1111/jpi.12542.
11. Jin, Y., Liu, Y., Xu, L., Xu, J., Xiong, Y., Peng, Y., Ding, K., Zheng, S., Yang, N., Zhang, Z., et al. (2022). Novel role for caspase 1 inhibitor VX765 in suppressing NLRP3 inflammasome assembly and atherosclerosis via promoting mitophagy and efferocytosis. Cell Death Dis. *13*, 512. https://doi.org/10.1038/s41419-022-04966-8.
12. Tong, M., Saito, T., Zhai, P., Oka, S.-I., Mizushima, W., Nakamura, M., Ikeda, S., Shirakabe, A., and Sadoshima, J. (2019). Mitophagy Is Essential for Maintaining Cardiac Function During High Fat Diet-Induced Diabetic Cardiomyopathy. Circ. Res. *124*, 1360–1371. https://doi.org/10.1161/CIRCRESAHA.118.314607.
13. Gong, Y., Luo, Y., Liu, S., Ma, J., Liu, F., Fang, Y., Cao, F., Wang, L., Pei, Z., and Ren, J. (2022). Pentacyclic triterpene oleanolic acid protects against cardiac aging through regulation of mitophagy and mitochondrial integrity. Biochim. Biophys. Acta, Mol. Basis Dis. *1868*, 166402. https://doi.org/10.1016/j.bbadis.2022.166402.
14. Yu, W., Wang, L., Ren, W.-Y., Xu, H.-X., Wu, N.N., Yu, D.-H., Reiter, R.J., Zha, W.-L., Guo, Q.-D., and Ren, J. (2024). SGLT2 inhibitor empagliflozin alleviates cardiac remodeling and contractile anomalies in a FUNDC1-dependent manner in experimental Parkinson's disease. Acta Pharmacol. Sin. *45*, 87–97. https://doi.org/10.1038/s41401-023-01144-0.
15. Dugbartey, G.J., Wonje, Q.L., Alornyo, K.K., Adams, I., and Diaba, D.E. (2022). Alpha-lipoic acid treatment improves adverse cardiac remodelling in the diabetic heart - The role of cardiac hydrogen sulfide-synthesizing enzymes. Biochem. Pharmacol. *203*, 115179. https://doi.org/10.1016/j.bcp.2022.115179.
16. Feng, J., Li, H., and Wang, S. (2022). Hydrogen sulfide alleviates uremic cardiomyopathy by regulating PI3K/PKB/mTOR-mediated overactive autophagy in 5/6 nephrectomy mice. Front. Pharmacol. *13*, 1027597. https://doi.org/10.3389/fphar.2022.1027597.
17. Li, Y., Liu, M., Song, X., Zheng, X., Yi, J., Liu, D., Wang, S., Chu, C., and Yang, J. (2020). Exogenous Hydrogen Sulfide Ameliorates Diabetic Myocardial Fibrosis by Inhibiting Cell Aging Through SIRT6/AMPK Autophagy. Front. Pharmacol. *11*, 1150. https://doi.org/10.3389/fphar.2020.01150.
18. Ji, L., Li, L., Qu, F., Zhang, G., Wang, Y., Bai, X., Pan, S., Xue, D., Wang, G., and Sun, B. (2016). Hydrogen sulphide exacerbates acute pancreatitis by over-activating autophagy via AMPK/mTOR pathway. J. Cell Mol. Med. *20*, 2349–2361. https://doi.org/10.1111/jcmm.12928.
19. Gao, J., Yu, L., Wang, Z., Wang, R., and Liu, X. (2020). Induction of mitophagy in C2C12 cells by electrical pulse stimulation involves increasing the level of the mitochondrial receptor FUNDC1 through the AMPK-ULK1 pathway. Am. J. Transl. Res. *12*, 6879–6894.
20. Karwi, Q.G., Bornbaum, J., Boengler, K., Torregrossa, R., Whiteman, M., Wood, M.E., Schulz, R., and Baxter, G.F. (2017). AP39, a mitochondria-targeting hydrogen sulfide (H2S) donor, protects against myocardial reperfusion injury independently of salvage kinase signalling. Br. J. Pharmacol. *174*, 287–301. https://doi.org/10.1111/bph.13688.
21. Yu, Y., Ye, S.-M., Liu, D.-Y., and Yang, L.-Q. (2021). AP39 ameliorates high fat diet-induced liver injury in young rats via alleviation of oxidative stress and mitochondrial impairment. Exp. Anim. *70*, 553–562. https://doi.org/10.1538/expanim.21-0056.
22. Marwah, M.K., Manhoosh, B., Shokr, H., Al Tahan, M.A., Stewart, R., Iqbal, M., Sanchez, L.D., Abdullah, S., Ahmad, S., Wang, K., et al. (2023). Transdermal delivery of mitochondrial-targeted hydrogen sulphide donor, AP39 protects against 6-hydroxydopamine-induced mitochondrial dysfunction. Eur. J. Pharm. Biopharm. *191*, 166–174. https://doi.org/10.1016/j.ejpb.2023.09.004.
23. Roth, G.A., Mensah, G.A., Johnson, C.O., Addolorato, G., Ammirati, E., Baddour, L.M., Barengo, N.C., Beaton, A.Z., Benjamin, E.J., Benziger, C.P., et al. (2020). Global Burden of Cardiovascular Diseases and Risk Factors, 1990-2019: Update From the GBD 2019 Study. J. Am. Coll. Cardiol. *76*, 2982–3021. https://doi.org/10.1016/j.jacc.2020.11.010.
24. Wang, W., Zhong, X., Fang, Z., Li, J., Li, H., Liu, X., Yuan, X., Huang, W., and Huang, Z. (2023). Cardiac sirtuin1 deficiency exacerbates ferroptosis in doxorubicin-induced cardiac injury through the Nrf2/Keap1 pathway. Chem. Biol. Interact. *377*, 110469. https://doi.org/10.1016/j.cbi.2023.110469.
25. She, G., Du, J.-C., Wu, W., Pu, T.-T., Zhang, Y., Bai, R.-Y., Zhang, Y., Pang, Z.-D., Wang, H.-F., Ren, Y.-J., et al. (2023). Hippo pathway activation mediates chemotherapy-induced anti-cancer effect and cardiomyopathy through causing mitochondrial damage and dysfunction. Theranostics *13*, 560–577. https://doi.org/10.7150/thno.79227.
26. Qin, D., Yue, R., Deng, P., Wang, X., Zheng, Z., Lv, M., Zhang, Y., Pu, J., Xu, J., Liang, Y., et al. (2021). 8-Formylophiopogonanone B antagonizes doxorubicin-induced

cardiotoxicity by suppressing heme oxygenase-1-dependent myocardial inflammation and fibrosis. Biomed. Pharmacother. *140*, 111779. https://doi.org/10.1016/j.biopha.2021.111779.

27. Li, Y., Chandra, T.P., Song, X., Nie, L., Liu, M., Yi, J., Zheng, X., Chu, C., and Yang, J. (2021). H2S improves doxorubicin-induced myocardial fibrosis by inhibiting oxidative stress and apoptosis via Keap1-Nrf2. Technol. Health Care *29*, 195–209. https://doi.org/10.3233/THC-218020.
28. Wang, J., Deng, B., Liu, Q., Huang, Y., Chen, W., Li, J., Zhou, Z., Zhang, L., Liang, B., He, J., et al. (2020). Pyroptosis and ferroptosis induced by mixed lineage kinase 3 (MLK3) signaling in cardiomyocytes are essential for myocardial fibrosis in response to pressure overload. Cell Death Dis. *11*, 574. https://doi.org/10.1038/s41419-020-02777-3.
29. Zhang, L., Jiang, Y.-H., Fan, C., Zhang, Q., Jiang, Y.-H., Li, Y., and Xue, Y.-T. (2021). MCC950 attenuates doxorubicin-induced myocardial injury in vivo and in vitro by inhibiting NLRP3-mediated pyroptosis. Biomed. Pharmacother. *143*, 112133. https://doi.org/10.1016/j.biopha.2021.112133.
30. Gu, J., Huang, H., Liu, C., Jiang, B., Li, M., Liu, L., and Zhang, S. (2021). Pinocembrin inhibited cardiomyocyte pyroptosis against doxorubicin-induced cardiac dysfunction via regulating Nrf2/Sirt3 signaling pathway. Int. Immunopharmacol. *95*, 107533. https://doi.org/10.1016/j.intimp.2021.107533.
31. Ye, B., Shi, X., Xu, J., Dai, S., Xu, J., Fan, X., Han, B., and Han, J. (2022). Gasdermin D mediates doxorubicin-induced cardiomyocyte pyroptosis and cardiotoxicity via directly binding to doxorubicin and changes in mitochondrial damage. Transl. Res. *248*, 36–50. https://doi.org/10.1016/j.trsl.2022.05.001.
32. Shao, D., Kolwicz, S.C., Wang, P., Roe, N.D., Villet, O., Nishi, K., Hsu, Y.-W.A., Flint, G.V., Caudal, A., Wang, W., et al. (2020). Increasing Fatty Acid Oxidation Prevents High-Fat Diet-Induced Cardiomyopathy Through Regulating Parkin-Mediated Mitophagy. Circulation *142*, 983–997. https://doi.org/10.1161/CIRCULATIONAHA.119.043319.
33. Ma, F., Li, H., Huo, H., Han, Q., Liao, J., Zhang, H., Li, Y., Pan, J., Hu, L., Guo, J., and Tang, Z. (2023). N-acetyl-L-cysteine alleviates FUNDC1-mediated mitophagy by regulating mitochondrial dynamics in type 1 diabetic nephropathy canine. Life Sci. *313*, 121278. https://doi.org/10.1016/j.lfs.2022.121278.
34. Wang, P., Wang, L., Lu, J., Hu, Y., Wang, Q., Li, Z., Cai, S., Liang, L., Guo, K., Xie, J., et al. (2019). SESN2 protects against doxorubicin-induced cardiomyopathy via rescuing mitophagy and improving mitochondrial function. J. Mol. Cell. Cardiol. *133*, 125–137. https://doi.org/10.1016/j.yjmcc.2019.06.005.
35. Zhou, J.-C., Jin, C.-C., Wei, X.-L., Xu, R.-B., Wang, R.-Y., Zhang, Z.-M., Tang, B., Yu, J.-M., Yu, J.-J., Shang, S., et al. (2023). Mesaconine alleviates doxorubicin-triggered cardiotoxicity and heart failure by activating PINK1-dependent cardiac mitophagy. Front. Pharmacol. *14*, 1118017. https://doi.org/10.3389/fphar.2023.1118017.
36. Liu, Z., Wang, M., Wang, X., Bu, Q., Wang, Q., Su, W., Li, L., Zhou, H., and Lu, L. (2022). XBP1 deficiency promotes hepatocyte pyroptosis by impairing mitophagy to activate mtDNA-cGAS-STING signaling in macrophages during acute liver injury. Redox Biol. *52*, 102305. https://doi.org/10.1016/j.redox.2022.102305.
37. Yu, X., Hao, M., Liu, Y., Ma, X., Lin, W., Xu, Q., Zhou, H., Shao, N., and Kuang, H. (2019). Liraglutide ameliorates non-alcoholic steatohepatitis by inhibiting NLRP3 inflammasome and pyroptosis activation via mitophagy. Eur. J. Pharmacol. *864*, 172715. https://doi.org/10.1016/j.ejphar.2019.172715.
38. Huang, H., Wang, T., Wang, L., Huang, Y., Li, W., Wang, J., Hu, Y., and Zhou, Z. (2023). Saponins of Panax japonicus ameliorates cardiac aging phenotype in aging rats by enhancing basal autophagy through AMPK/mTOR/ULK1 pathway. Exp. Gerontol. *182*, 112305. https://doi.org/10.1016/j.exger.2023.112305.
39. Hung, C.-M., Lombardo, P.S., Malik, N., Brun, S.N., Hellberg, K., Van Nostrand, J.L., Garcia, D., Baumgart, J., Diffenderfer, K., Asara, J.M., and Shaw, R.J. (2021). AMPK/ULK1-mediated phosphorylation of Parkin ACT domain mediates an early step in mitophagy. Sci. Adv. *7*, eabg4544. https://doi.org/10.1126/sciadv.abg4544.
40. Chen, C., Jiang, L., Zhang, M., Pan, X., Peng, C., Huang, W., and Jiang, Q. (2019). Isodunnianol alleviates doxorubicin-induced myocardial injury by activating protective autophagy. Food Funct. *10*, 2651–2657. https://doi.org/10.1039/c9fo00063a.
41. Shen, Y., Liu, W.-W., Zhang, X., Shi, J.-G., Jiang, S., Zheng, L., Qin, Y., Liu, B., and Shi, J.-H. (2020). TRAF3 promotes ROS production and pyroptosis by targeting ULK1 ubiquitination in macrophages. FASEB J *34*, 7144–7159. https://doi.org/10.1096/fj.201903073R.
42. Cai, C., Guo, Z., Chang, X., Li, Z., Wu, F., He, J., Cao, T., Wang, K., Shi, N., Zhou, H., et al. (2022). Empagliflozin attenuates cardiac microvascular ischemia/reperfusion through activating the AMPKα1/ULK1/FUNDC1/mitophagy pathway. Redox Biol. *52*, 102288. https://doi.org/10.1016/j.redox.2022.102288.
43. Zhang, S., Shen, J., Zhu, Y., Zheng, Y., San, W., Cao, D., Chen, Y., and Meng, G. (2023). Hydrogen sulfide promoted retinoic acid-related orphan receptor α transcription to alleviate diabetic cardiomyopathy. Biochem. Pharmacol. *215*, 115748. https://doi.org/10.1016/j.bcp.2023.115748.
44. Nie, L., Liu, M., Chen, J., Wu, Q., Li, Y., Yi, J., Zheng, X., Zhang, J., Chu, C., and Yang, J. (2021). Hydrogen sulfide ameliorates doxorubicin-induced myocardial fibrosis in rats via the PI3K/AKT/mTOR pathway. Mol. Med. Rep. *23*, 299. https://doi.org/10.3892/mmr.2021.11938.
45. Kar, S., Shahshahan, H.R., Hackfort, B.T., Yadav, S.K., Yadav, R., Kambis, T.N., Lefer, D.J., and Mishra, P.K. (2019). Exercise Training Promotes Cardiac Hydrogen Sulfide Biosynthesis and Mitigates Pyroptosis to Prevent High-Fat Diet-Induced Diabetic Cardiomyopathy. Antioxidants *8*, 638. https://doi.org/10.3390/antiox8120638.
46. Yang, T., Yang, Q., Lai, Q., Zhao, J., Nie, L., Liu, S., Yang, J., and Chu, C. (2023). AP39 inhibits ferroptosis by inhibiting mitochondrial autophagy through the PINK1/parkin pathway to improve myocardial fibrosis with myocardial infarction. Biomed. Pharmacother. *165*, 115195. https://doi.org/10.1016/j.biopha.2023.115195.
47. Hao, J., Xi, Y., Jiao, L., Wen, X., Wu, R., Chang, G., Sun, F., Wei, C., and Li, H. (2022). Exogenous hydrogen sulfide inhibits the senescence of cardiomyocytes through modulating mitophagy in rats. Cell. Signal. *100*, 110465. https://doi.org/10.1016/j.cellsig.2022.110465.
48. Nguyen, T.T.P., Kim, D.-Y., Lee, Y.-G., Lee, Y.-S., Truong, X.T., Lee, J.-H., Song, D.-K., Kwon, T.K., Park, S.-H., Jung, C.H., et al. (2021). SREBP-1c impairs ULK1 sulfhydration-mediated autophagic flux to promote hepatic steatosis in high-fat-diet-fed mice. Mol. Cell *81*, 3820–3832.e7. https://doi.org/10.1016/j.molcel.2021.06.003.
49. Patel, D., Yadav, P., Singh, S.K., Tanwar, S.S., Sehrawat, A., Khurana, A., Bhatti, J.S., and Navik, U. (2024). Betaine alleviates doxorubicin-induced nephrotoxicity by preventing oxidative insults, inflammation, and fibrosis through the modulation of Nrf2/HO-1/NLRP3 and TGF-β expression. J. Biochem. Mol. Toxicol. *38*, e23559. https://doi.org/10.1002/jbt.23559.
50. Dhingra, R., Rabinovich-Nikitin, I., Rothman, S., Guberman, M., Gang, H., Margulets, V., Jassal, D.S., Alagarsamy, K.N., Dhingra, S., Valenzuela Ripoll, C., et al. (2022). Proteasomal Degradation of TRAF2 Mediates Mitochondrial Dysfunction in Doxorubicin-Cardiomyopathy. Circulation *146*, 934–954. https://doi.org/10.1161/CIRCULATIONAHA.121.058411.
51. Zhao, F.-L., Fang, F., Qiao, P.-F., Yan, N., Gao, D., and Yan, Y. (2016). AP39, a Mitochondria-Targeted Hydrogen Sulfide Donor, Supports Cellular Bioenergetics and Protects against Alzheimer's Disease by Preserving Mitochondrial Function in APP/PS1 Mice and Neurons. Oxid. Med. Cell. Longev *2016*, 8360738. https://doi.org/10.1155/2016/8360738.
52. Ni, J., Jiang, L., Shen, G., Xia, Z., Zhang, L., Xu, J., Feng, Q., Qu, H., Xu, F., and Li, X. (2021). Hydrogen sulfide reduces pyroptosis and alleviates ischemia-reperfusion-induced acute kidney injury by inhibiting NLRP3 inflammasome. Life Sci. *284*, 119466. https://doi.org/10.1016/j.lfs.2021.119466.
53. Wen, Y., Wu, J., Pu, Q., He, X., Wang, J., Feng, J., Zhang, Y., Si, F., Wen, J.G., and Yang, J. (2023). ABT-263 exerts a protective effect on upper urinary tract damage by alleviating neurogenic bladder fibrosis. Ren. Fail. *45*, 2194440. https://doi.org/10.1080/0886022X.2023.2194440.
54. Li, Y., Qin, W., Liang, Q., Zeng, J., Yang, Q., Chen, Y., Wang, J., and Lu, W. (2023). Bufei huoxue capsule alleviates bleomycin-induced pulmonary fibrosis in mice via TGF-β1/Smad2/3 signaling. J. Ethnopharmacol. *316*, 116733. https://doi.org/10.1016/j.jep.2023.116733.
55. Zhang, X., Qu, H., Yang, T., Liu, Q., and Zhou, H. (2022). Astragaloside IV attenuate MI-induced myocardial fibrosis and cardiac remodeling by inhibiting ROS/caspase-1/GSDMD signaling pathway. Cell Cycle *21*, 2309–2322. https://doi.org/10.1080/15384101.2022.2093598.
56. Nicholson, C.K., Lambert, J.P., Molkentin, J.D., Sadoshima, J., and Calvert, J.W. (2013). Thioredoxin 1 is essential for sodium sulfide-mediated cardioprotection in the setting of heart failure. Arterioscler. Thromb. Vasc. Biol. *33*, 744–751. https://doi.org/10.1161/ATVBAHA.112.300484.

57. Zhou, X., Zhao, L., Mao, J., Huang, J., and Chen, J. (2015). Antioxidant effects of hydrogen sulfide on left ventricular remodeling in smoking rats are mediated via PI3K/Akt-dependent activation of Nrf2. Toxicol. Sci. *144*, 197–203. https://doi.org/10.1093/toxsci/kfu272.

58. Fox, B.C., Slade, L., Torregrossa, R., Pacitti, D., Szabo, C., Etheridge, T., and Whiteman, M. (2021). The mitochondria-targeted hydrogen sulfide donor AP39 improves health and mitochondrial function in a C. elegans primary mitochondrial disease model. J. Inherit. Metab. Dis. *44*, 367–375. https://doi.org/10.1002/jimd.12345.

59. Zhang, M., Wei, L., Xie, S., Xing, Y., Shi, W., Zeng, X., Chen, S., Wang, S., Deng, W., and Tang, Q. (2021). Activation of Nrf2 by Lithospermic Acid Ameliorates Myocardial Ischemia and Reperfusion Injury by Promoting Phosphorylation of AMP-Activated Protein Kinase α (AMPKα). Front. Pharmacol. *12*, 794982. https://doi.org/10.3389/fphar.2021.794982.

60. Han, Y., Xiong, S., Zhao, H., Yang, S., Yang, M., Zhu, X., Jiang, N., Xiong, X., Gao, P., Wei, L., et al. (2021). Lipophagy deficiency exacerbates ectopic lipid accumulation and tubular cells injury in diabetic nephropathy. Cell Death Dis. *12*, 1031. https://doi.org/10.1038/s41419-021-04326-y.

STAR★METHODS

KEY RESOURCES TABLE

REAGENT or RESOURCE	SOURCE	IDENTIFIER
Antibodies		
Anti-CSE	Proteintech	Cat# 12217-1-AP, RRID:AB_2087497
Anti-α-SMA	Proteintech	Cat# 14395-1-AP, RRID:AB_2223009
Anti-CollagenIII	Proteintech	Cat# 22734-1-AP, RRID:AB_2879158
Anti-MMP8	Proteintech	Cat# 17874-1-AP, RRID:AB_2144582
Anti-MMP13	Proteintech	Cat# 18165-1-AP, RRID:AB_2144858
Anti-TIMP1	Proteintech	Cat# 16644-1-AP, RRID:AB_2878292
Anti-Caspase1	Proteintech	Cat# 22915-1-AP, RRID:AB_2876874
Anti-IL-1β	Proteintech	Cat# 16806-1-AP, RRID:AB_10646432
Anti-Beclin1	Proteintech	Cat# 11306-1-AP, RRID:AB_2259061
Anti-LC3	Proteintech	Cat# 18725-1-AP, RRID:AB_2137745
Anti-P62	Proteintech	Cat# 18420-1-AP, RRID:AB_10694431
Anti-AMPK	Proteintech	Cat# 10929-2-AP, RRID:AB_2169568
Anti- ULK1	Proteintech	Cat# 20986-1-AP, RRID:AB_2878783
Anti-*p*-AMPK	Cell Signaling Technology	Cat# 2535 (also 2535S, 2535L, 2535P), RRID:AB_331250
Anti-GSDMD	Cell Signaling Technology	Cat# 39754, RRID:AB_2916333
Anti-NLRP3	Cell Signaling Technology	Cat# 15101, RRID:AB_2722591
Anti- *p*-ULK1	Abcam	Cat# ab133747, RRID:AB_3073515
Anti-FUNDC1	Thermo Scientific	Cat# PA5-75706, RRID:AB_2719434
goat anti-mouse IgG-HRP	Proteintech	Cat# SA00001-1, RRID:AB_2722565
goat anti-rabbit IgG-HRP	Proteintech	Cat# SA00001-2, RRID:AB_2722564
Anti-GAPDH	Proteintech	Cat# 60004-1-Ig, RRID:AB_2107436
Chemicals, peptides, and recombinant proteins		
Doxorubicin hydrochloride	Med Chem Express	Cat# HY-15142
AP39	Med Chem Express	Cat# HY-126124
PAG	Sigma-Aldrich	Cat# P7888
Dorsomorphin	Med Chem Express	Cat# HY-13418A
SBI-0206965	Med Chem Express	Cat# HY-16966
Critical commercial assays		
H_2S content kit	Grace Biotechnology	Cat# G0133W
JC-1 kit	Beyotime	Cat# C2003S
Total Reactive Oxygen Species (ROS) Assay Kit	Beyotime	Cat# S0033S
Mito-HS Assay Kit	KEAN Biotechnology	N/A
Deposited data		
Original blot data	Mendeley data	https://doi.org/10.17632/kx2r4dms4j.1
Experimental models: Cell lines		
H9c2	ATCC	Cat# 60096, RRID:CVCL_0286
Experimental models: Organisms/strains		
Sprague-Dawley rats	Changsha Tianqin Biotechnology Co	http://cstqsw.com/mobile/index.html

(*Continued on next page*)

Continued

REAGENT or RESOURCE	SOURCE	IDENTIFIER
Oligonucleotides		
Primer: GAPDH_F: ACAGCAACAGGGTGGTGGAC	Sangon Biotech Co	https://www.sangon.com/
Primer: GAPDH_ R: TTTGAGGGTGCAGCGAACTT	Sangon Biotech Co	https://www.sangon.com/
Primer: IL-1β_F: CAGCAGCATCTCGACAAGAG	Sangon Biotech Co	https://www.sangon.com/
Primer: IL-1β_ R: AAAGAAGGTGCTTGGGTCCT	Sangon Biotech Co	https://www.sangon.com/
Primer: P62_F: AGCATACAGAGAGCACCCAT	Sangon Biotech Co	https://www.sangon.com/
Primer: P62_ R: ACATACAGAAGCCAGAATGCAG	Sangon Biotech Co	https://www.sangon.com/
Primer: GSDMDβ_F: TTAGTCTGCTTGCCGTACTCC	Sangon Biotech Co	https://www.sangon.com/
Primer: GSDMD_ R: GTCCTGTAAAATCCTCCCGATG	Sangon Biotech Co	https://www.sangon.com/
Primer: Col2a1_F: GGCCAGGATGCCCGAAAATTA	Sangon Biotech Co	https://www.sangon.com/
Primer: Col2a1_ R: ACCCCTCTCTCCCTTGTCAC	Sangon Biotech Co	https://www.sangon.com/
Software and algorithms		
BIO-RAD XRS+ imaging system	BIO-RAD Life Science	N/A
ImageJ	NIH	https://imagej.net/ij/
GraphPad Prism V9.5.1	GraphPad software	https://www.graphpad.com/

RESOURCE AVAILABILITY

Lead contact

Further information and requests for resources and reagents should be directed to and will be fulfilled by the corresponding author, Prof. Dr. Jun Yang(2018010473@usc.edu.cn).

Materials availability

This study did not generate new unique reagents.

Date and code availability

- The dataset is publicly available as of the date of publication.
- This study did not report the original code.
- Any additional information required to reanalyze the data reported in this study is available from the lead contact upon request

EXPERIMENTAL MODEL AND STUDY PARTICIPANT DETAILS

Animal experiments

This experiment was approved by the University of South China Animal Ethics Committee (Granted ID: USC201910XS006) and conducted in compliance with the Laboratory Animal Regulations and Laboratory Animal Welfare Regulations of China. Rats were housed in an SPF environment at 23°C and 60% humidity, with free access to food and water and light/dark lighting alternating every 12 h. Doxorubicin hydrochloride was used to establish doxorubicin-induced myocardial fibrosis in model rats. Doxorubicin hydrochloride, AP39, and PAG solution were used in this experiment. Rats were randomly divided into six groups (n = 10): control, DOX, DOX+AP39, DOX+AP39+PAG, AP39, and DMSO groups.

In vitro studies

H9c2 cell line was purchased from ATCC (Manassas, VA, USA), cultured in high glucose DMEM (Gibco, Grand Island, USA) medium containing 10% FBS, 1% penicillin/streptomycin at 37°C and 5% CO_2 in a humidified atmosphere. The medium was refreshed every two days and processed for replication when the cell density reached 80%. Doxorubicin hydrochloride, AP39, PAG, AMPK inhibitor dorsomorphin, and ULK1 inhibitor SBI-0206965 were performed in the vitro experiment.

METHOD DETAILS

Animal

After one week of adaptation feeding, a total 60 male rats aged 8 weeks and weighing (200 ± 20)g were randomly divided into six groups (n = 10): control, DOX, DOX+AP39, DOX+AP39+PAG, AP39, and DMSO groups. Intraperitoneal injection of doxorubicin hydrochloride solution

(5 mg/kg/week, Med Chem Express, New Jersey, USA, HY-15142) was performed as described in the literature[29,49,50] for four weeks (cumulative dose: 20 mg/kg) in rats from the DOX, DOX+AP39, and DOX+AP39+PAG groups. The control, AP39, and DMSO groups were injected intraperitoneally with equal doses of saline. After four weeks, rats in the DOX+AP39, AP39, and DOX+AP39+PAG groups were given intraperitoneal administration of AP39[51] (100 nM/kg/d 0.05% DMSO dissolved, Med Chem Express, New Jersey, USA, HY-126124). At the same time, rats in the DOX+AP39+PAG group were given simultaneous intraperitoneal administration of the endogenous hydrogen sulfide-generating enzyme inhibitor PAG[52] (50 mg/kg/d, Sigma-Aldrich, Missouri, MO, USA, P7888). Rats in the DOX and control groups were given equal amounts of saline intervention, and rats in the DMSO group were given equal amounts of 0.05% DMSO (Sigma-Aldrich, Missouri, USA, D2650) for four weeks. No new rats were enrolled in the follow-up study when the rats died during the model-establishment period. Rats underwent euthanasia by carbon dioxide asphyxiation, followed by cervical dislocation at the end of the experiment.

Echocardiography

At the end of the drug intervention period, the rats were anesthetized with 2.5% isoflurane (RWD Life Science, Shenzhen, China, R510-22-10), followed by an anesthetic respiratory system (1.5% isoflurane to maintain anesthesia), an ultrasound machine (GE Versana Premier), and L8-18i-RS ultrahigh-frequency line-array probe were performed to measure LVEDd (Left Ventricular end Diastolic Diameter), LVESd (Left Ventricular End-Systolic Diameter), and the corresponding LVFS (left ventricular fractional shortening, LVFS = [LVEDd−LVESd/LVEDD]×100) from the left parasternal axis using two-dimensional echocardiography for five consecutive cardiac cycles.

HW/BW

The rats were weighed (body weight, BW) before euthanasia. The hearts were collected and washed with cold PBS. Heart weight (HW) and HW/BW values were measured after euthanasia.

Masson staining

The isolated rat hearts were fixed in 4% paraformaldehyde, rinsed in hydrogen peroxide, dehydrated in anhydrous ethanol, embedded in paraffin, prepared into 4 μm-sized sections, baked, dewaxed, and stained for 3–5 min. Then, the hearts were rinsed using tap and distilled water, stained according to the instructions of the Masson staining kit (Abiowell, Changsha, China, AWI0253a), and sealed. Then, the staining was observed under a microscope. Five fields of view were randomly selected from each sample.[53,54]

HE staining

Isolated rat hearts were fixed using 4% paraformaldehyde, dehydrated, and paraffin-embedded to make 4 μm thin sections. Next, the samples were dewaxed and stained with hematoxylin and eosin dyes (Beyotime Biotechnology Co., Ltd., Shanghai, China, C0105S), respectively, sealed, and fixed using alcohol dehydration. Next, the stained samples were observed under a microscope. Five fields of view were randomly selected from each sample.[54]

Immunohistochemical staining

Paraffin-embedded tissue sections were dewaxed and washed with water, then restored with antigen and closed with appropriate proportions of goat serum. Collagen Type III Polyclonal antibody (1:400, Proteintech, Chicago, USA, 22734-1-AP) was added and incubated overnight at 4°C. The sections were washed and incubated with Biotin-conjugated Affinipure Goat Anti-Rabbit IgG (1:500, Proteintech, Chicago, USA, SA00004-2) the next day. The sections were rinsed, incubated with Biotin-conjugated Affinipure Goat Anti-Rabbit IgG (1:500, Proteintech, Chicago, USA, SA00004-2), washed, visualized, dehydrated, sealed, and observed under a microscope in five randomly selected fields of view from each sample.[46,55]

Transmission electron microscopy

The myocardial tissues were fixed with 2.5% glutaraldehyde and cut into 50–100 nm thin sections, and phosphoric acid rinsing solution (Beyotime Institute of Biotechnology, Shanghai, China) was used. After being immersed in 1% osmium tetroxide (Absin Biosciences, Inc., Shanghai, China), the tissues were fixed and rinsed with phosphoric acid, followed by gradient acetone immersion. After dehydrating and drying, the tissues were stained with 3% uranyl acetate and lead nitrate for 10–20 min and rinsed with distilled water. The ultrastructure was observed under transmission electron microscopy.

Construction of the protein–protein interaction (PPI) network

The STRING database (https://cn.string-db.org/) was used to analyze the interaction among AMPK, ULK1, and FUNDC1. The "*Homo sapiens*" organism was performed in the PPI network. The output results of "FUNDC1" and "AMPK–ULK1–FUNDC1" were saved to evaluate their interactions.

Myocardial H_2S content testing

The myocardial levels of H_2S were determined by the Methylene Blue method.[56,57] The sample was prepared according to the requirements of the H_2S kit (Grace Biotechnology, Suzhou, China, G0133W). Next, it was centrifuged at 12,000 RPM for 10 min at 4°C. The supernatant was extracted, and reagents 1 and 2 were added according to the instructions. Then, the sample was mixed and incubated at room temperature for 15 min. Next, absorption was measured at 665 nm. The corresponding H_2S content was calculated according to the formula: H_2S (μmol/g fresh weight) = (△A + 0.0014) ÷ 7.6577 ÷ (V1 ÷ V × W) = 0.82 × (△A + 0.0014) ÷ W, in which V - added to the volume of the extraction solution, 1 mL; V1 - the volume of the sample in the reaction, 0.16 mL; W —— sample weight, g; △A = A measurement - A Blank (A is the absorbance value read at 665 nm).

Cell culture

The H9c2 cardiomyocyte cell line was purchased from ATCC (Manassas, VA, USA) and cultured in high glucose DMEM (Gibco, Grand Island, USA) medium containing 10% FBS, 1% penicillin/streptomycin at 37°C and 5% CO2. The medium was refreshed every two days and processed for replication when the cell density reached 80%, and when the cell number reached 1×10^6, cells were inoculated in 6-well plates. The cells were assigned to the control, DOX, DOX+AP39, DOX+AP39+PAG, AP39, and DMSO groups. DOX, DOX+AP39, and DOX+AP39+PAG groups were given 1 μM DOX[29] (Med Chem Express, New Jersey, USA, HY-15142) intervention treatment. The DOX+AP39, DOX+AP39+PAG, and AP39 control groups were given 100 nM AP39[58] (Med Chem Express, New Jersey, USA, HY-126124) pretreatment for 0.5 h. In contrast, the DOX+AP39+PAG group was given 1 mM PAG[52] (Sigma-Aldrich, Missouri, USA, P7888). The pretreatment stage lasted 0.5 h, and the DMSO group was given equal amounts of DMSO for 24 h. To investigate whether AP39 exerts a regulatory effect on the AMPK–ULK1–FUNDC1 pathway and its impact on physiological effects on cardiomyocytes, we administered the AMPK inhibitor dorsomorphin[59] (10 μM, Med Chem Express, New Jersey, USA, HY-13418A) in advance of the AP39 intervention in DOX-treated cells. ULK1 inhibitor SBI-0206965[60] (10uM, Med Chem Express, New Jersey, USA, HY-16966) was pretreated for 0.5 h to investigate whether AP39 regulates FUNDC1-mediated mitophagy via AMPK–ULK1 and thus inhibits DOX-induced cardiomyocyte pyroptosis occurrence.

RT-qPCR

Total RNA was extracted from the rat myocardial tissue or cellular using TRIzol (Thermal, USA) and transcribed into cDNA with the PrimeScriptTM RT kit (Takara, Japan). Real-time qPCR was performed with SYBR green (Takara, Japan) under standard conditions of 95°C for 30 s, 40 cycles of 95°C for 5 s, and 60°C for 30 s. Real-time qPCR was conducted under standard conditions, *GAPDH* was used as an internal reference, and the relative expression levels of target genes were obtained using the $2^{-\Delta\Delta Ct}$ method. The primer sequences are presented as follows:

R-*GAPDH*： F: ACAGCAACAGGGTGGTGGAC.
R: TTTGAGGGTGCAGCGAACTT.
R-*IL-1β*： F: CAGCAGCATCTCGACAAGAG.
R: AAAGAAGGTGCTTGGGTCCT.
R-*P62*： F: AGCATACAGAGAGCACCCAT.
R: ACATACAGAAGCCAGAATGCAG.
R-*GSDMD*： F: TTAGTCTGCTTGCCGTACTCC.
R: GTCCTGTAAAATCCTCCCGATG.
R-*Col2a1*： F: GGCCAGGATGCCCGAAAATTA.
R: ACCCCTCTCTCCCTTGTCAC.

Mito-HS mitochondrial H_2S fluorescent probe assay

The cells were washed three times with PBS at the end of the drug intervention and incubated for 1 h in an incubator with 10 μM Mito-HS (KEAN Biotechnology, Nanjing, China) in PBS solution with 30% DMSO according to the instructions. Next, the sample was washed three times with PBS at the end of incubation. The fluorescent signal was observed under a fluorescent microscope.[46]

Mitochondrial membrane potential detection

After the drug intervention, the cells were washed once with cold PBS, 1 mL cell culture medium, and 1 mL JC-1 staining buffer (Beyotime, Shanghai, China, C2003S). The cells were then added according to the kit instructions, mixed, and incubated for 20 min at 37°C in an incubator. The supernatant was discarded, and the JC-1 staining buffer was washed twice. A 2 mL cell culture medium was added, and the fluorescence signal was observed under a fluorescence microscope.

Cellular reactive oxygen species detection

Cells were washed three times with cold PBS at the end of the drug intervention. According to the kit instructions, DCFH-DA (10 μM, Beyotime, Shanghai, China, S0033S) was diluted in a serum-free medium and incubated for 20 min at 37°C. After incubation, the cells were washed three times with serum-free medium and observed under a fluorescent microscope.

Western blot

Myocardial tissue or cellular proteins were extracted using a protease inhibitor-containing cell lysate. Protein quantification was performed using a BCA quantification kit (Beyotime, Shanghai, China, P0010S). After equalization of protein concentrations, an appropriate amount of protein loading buffer was added, and the proteins were denatured by heating at 95° for 10 min and separated by 10–12% SDS-PAGE. The proteins were wet transferred to PVDF membranes and blocked with a 5% fat-free milk-blocking solution for 1 h. CSE (12217-1-AP), α-SMA (14395-1-AP), collagen III (22734-1-AP), MMP8 (17874-1-AP), MMP13 (18165-1-AP), TIMP1 (6644- 1-AP), caspase1 (22915-1-AP), IL-1β (16806-1-AP), beclin1 (11306-1-AP), LC3 (18725-1-AP), P62 (18420-1-AP), AMPK (10929-2-AP), ULK1 (20986-1-AP), and GAPDH (60004-1-IG) were purchased from Proteintech (Chicago, USA). *p*-AMPK (2535), GSDMD (39754), and NLRP3 (15101) were purchased from CST (Cell Signaling Technology, Boston, MA, USA). *p*-ULK1 (ab133747) primary antibody was purchased from Abcam (Cambridge, UK). FUNDC1 (PA5-75706) primary antibody was purchased from Thermofish (Thermo Scientific, Massachusetts, USA). Mouse (SA00001-1)/rabbit(SA00001-2) secondary antibodies were purchased from Proteintech (Chicago, US).

The primary antibody was incubated overnight at 4°, then washed 10 min × 3 times with TBST. The secondary antibodies of the related species were incubated for 1 h at room temperature, washed again for 10 min × 3 times with TBST, and photographed using ECL solution. The images were obtained using the BIO-RAD XRS+ imaging system (BIO-RAD Life Science, California, USA). The comparative data were analyzed using ImageJ software (NIH, Bethesda, USA), and GAPDH was used as an internal reference to calculate the relative values of each protein.

QUANTIFICATION AND STATISTICAL ANALYSIS

Statistical analysis

Values are presented as the mean ± standard deviation for data normally distributed or median and interquartile range for data not normally distributed for continuous variables and number (%) for categorical variables. The representative image for each group was selected based on the mean value after the quantitative analysis. Statistical analyses were performed with GraphPad Prism software (version 9.5.1). For comparisons of the two groups, the Student's *t* test was used. A one-way analysis of variance was used with Bonferroni's or Dunnett's multiple-comparisons test for normally distributed data or the Mann–Whitney test for non-normally distributed data for comparisons of more than two groups. Unless stated otherwise, $p < 0.05$ was considered statistically significant.